Journal of Medicinal Chemistry



Article

# Development of 1,2,4-Oxadiazoles as Potent and Selective Inhibitors of the Human Deacetylase Sirtuin 2: Structure-Activity Relationship, X-Ray Crystal Structure and Anticancer Activity

Sebastien Moniot, Mariantonietta Forgione, Alessia Lucidi, Gebremedhin Solomon Hailu, Angela Nebbioso, Vincenzo Carafa, Francesca Baratta, Lucia Altucci, Nicola Giacchè, Daniela Passeri, Roberto Pellicciari, Antonello Mai, Clemens Steegborn, and Dante Rotili

*J. Med. Chem.*, **Just Accepted Manuscript** • DOI: 10.1021/acs.jmedchem.6b01609 • Publication Date (Web): 27 Feb 2017



ACS Publications

Journal of Medicinal Chemistry is published by the American Chemical Society. 1155 Sixteenth Street N.W., Washington, DC 20036

# Development of 1,2,4-Oxadiazoles as Potent and Selective Inhibitors of the Human Deacetylase Sirtuin 2: Structure-Activity Relationship, X-Ray Crystal Structure and Anticancer Activity

Sébastien Moniot,[†,¶] Mariantonietta Forgione,[§,£,¶] Alessia Lucidi,[§] Gebremedhin S. Hailu,[§] Angela Nebbioso,[#] Vincenzo Carafa,[#] Francesca Baratta,[#] Lucia Altucci,[#] Nicola Giacché,[°] Daniela Passeri,[°] Roberto Pellicciari,[°] Antonello Mai,*[,§] Clemens Steegborn,*[,†] Dante Rotili*[,§]

[†]Department of Biochemistry and Research Center for Bio-Macromolecules, University of Bayreuth, 95440 Bayreuth, Germany

[§]Department of Drug Chemistry and Technologies, Sapienza University of Rome, P. le A. Moro 5, 00185 Rome, Italy, Laboratory affiliated to Istituto Pasteur Italia – Fondazione Cenci Bolognetti

[£]Center for Life Nano Science@Sapienza, Istituto Italiano di Tecnologia, Viale Regina Elena, 291, 00161 Rome, Italy

[#]Department of Biochemistry, Biophysics and General Pathology, Second University of Naples, Vico L. De Crecchio 7, 80138 Naples, Italy

[°]TES Pharma S.r.l. Via P. Togliatti 20, 06073 Corciano Perugia, Italy

[¶]These authors contributed equally to this work.

**ABSTRACT**

Sirt2 is a target for the treatment of neurological, metabolic and age-related diseases including cancer. Here we report a series of Sirt2 inhibitors based on the 1,2,4-oxadiazole scaffold. These compounds are potent Sirt2 inhibitors active at single-digit μM level by using the Sirt2 substrate α-tubulin-acetylLys40 peptide, and inactive up to 100 μM against Sirt1, -3 and -5 (deacetylase and desuccinylase activities). Their mechanism of inhibition is uncompetitive towards both the peptide substrate and $NAD^+$, and the crystal structure of a 1,2,4-oxadiazole analog in complex with Sirt2 and ADP-ribose reveals its orientation in a still unexplored sub cavity useful for further inhibitor development. Tested in leukemia cell lines, **35** and **39** induced apoptosis and/or showed antiproliferative effects at 10 or 25 μM after 48 h. Western blot analyses confirmed the involvement of Sirt2 inhibition for their effects in NB4 and in U937 cells. Our results provide novel Sirt2 inhibitors with a compact scaffold and structural insights for further inhibitor improvement.

## INTRODUCTION

Sirtuins are a family of $NAD^+$-dependent lysine deacylases highly conserved from bacteria to humans. In mammals there are seven members, Sirt1-7, that localize in different subcellular compartments, such as cytoplasm (Sirt1 and Sirt2), nucleus (Sirt1, Sirt2, Sirt6, and Sirt7) and mitochondria (Sirt3, Sirt4 and Sirt5). All sirtuins share a conserved $NAD^+$-binding and catalytic core domain, but possess distinct *N*- or *C*-terminal extensions.[1-3] Initially reported to be ADP-ribosyltransferases and/or deacetylases acting on acetyl-lysine substrates from both histones and non-histone proteins, some of them are now known to remove other acyl (malonyl, glutaryl, succinyl, myristoyl) rather than acetyl groups from protein lysines.[4-6] Due to this multifaceted activity on various substrate proteins, sirtuins are involved in many biological processes, including transcriptional regulation, genome stability, metabolic regulation, and cell survival.[7-9]

Sirt2 is primarily localized in the cytoplasm and strongly expressed in neuronal tissue, where it contributes to protection against oxidative stress and memory function.[10-12] Sirt2 is also expressed in many other tissues and can transiently translocate to the nucleus during G2/M transition. Here it deacetylates histone H4K16 thus modulating chromatin condensation during metaphase.[13] Sirt2 regulates mitosis also through deacetylation of α-tubulin, and is linked with cancer metabolism by interaction with p65, FOXO1, FOXO3, and HIF-1α.[14-17] The exact role of Sirt2 in cancer is controversial, as for other sirtuins (Sirt1, Sirt3, Sirt6). Sirt2 has been suggested to be a tumor suppressor because Sirt2-knockout mice developed spontaneous tumors in multiple organs, probably due to a Sirt2 loss-mediated deregulation of the anaphase-promoting complex/cyclosome activity, leading to increased levels of the mitotic death factors Aurora-A and -B.[18] Such tumor development may be also due to higher genomic instability and chromosomal aberrations, as a result of reduction of both the mitotic deposition of H4K20me1 and the levels of the related histone

methyltransferase PR-Set7 after Sirt2 depletion.[19] On the other hand, analyses of Sirt2 expression in human cancer samples produced contradictory results, and Sirt2 knockdown or Sirt1/Sirt2 pharmacological inhibition repressed cancer cell proliferation, through activation and/or accumulation of tumor suppressor proteins such as p53[20] or FOXO1,[21] or through destabilization of oncoproteins such as c-Myc and K-RAS.[22-24] In breast cancer, Sirt2 is the predominant sirtuin and appears to act as a tumor suppressor or tumor promoter depending on the breast tumor grade.[25] Finally, the overexpression of Sirt2 attenuated drug sensitivity and led to multidrug resistance in acute myeloid leukemia (AML) through increased expression of phosphorylated ERK1/2,[26] and has been recently reported as a novel and unfavorable prognostic biomarker in AML patients.[27]

A number of Sirt2-selective inhibitors have been described so far: AGK2 (**1**),[28] AK-7,[29] MIND4,[30] SirReal2 (**2**)[31] and its analogues,[32] the 4-chromanone compound **6f**,[33] the benzamide analog **17k**,[34] the nicotinamide derivatives **33i**[35] and **64**[36] and analogues,[37] ICL-SIRT078,[38] the macrocyclic peptide S2iL5 (**3**),[39] and the thiomyristoyl peptide TM[23] (Figure 1). However, various shortcomings such as limited solubility or bioavailability or failures to further improve these mostly large compounds lead to a requirement of further Sirt2 inhibitor scaffolds. Furthermore, while their capability to exert neuroprotective effects in cellular models of neurodegenerative diseases has mostly been reported, the anticancer properties of Sirt2 inhibitors are little studied.

Insert Figure 1

In our previous attempt to identify potent and isoform-selective sirtuin inhibitors, we docked a library of structurally diverse compounds in the crystal structures of Sirt2, -3, -5 and -6.[40] This study yielded two potent and Sirt2 selective inhibitors, but their compound scaffolds were not suitable for cellular applications (see Figure S1 in Supporting Information). We thus used one of the

less potent but already Sirt2-selective compounds from this screen, the 3,5-disubstituted 1,2,4-oxadiazole CSC37[40] (**4**), as the starting point for development of novel Sirt2 inhibitors. Extensive structure-activity relationship (SAR) studies have been applied on the 3-(4-chlorophenyl)-5-(piperidin-1-ylmethyl)-1,2,4-oxadiazole **4** to obtain new hit compounds showing potent and highly selective inhibition of Sirt2 in vitro (Figure 2). In particular, the influence of the *p*-chloro substitution at the C3-phenyl ring of **4** has been evaluated by shifting the chloro atom from *para* to *meta* or *ortho* position, and by removing it or by replacing the phenyl with a 3-pyridyl ring (compounds **5**-**8**). The piperidinyl moiety has been removed or replaced with smaller or bigger amines (compounds **9**-**12**), or with morpholine, thiomorpholine, *N*-methyl- or *N*-phenylpiperazine moieties carrying an additional heteroatom in their structures (compounds **13**-**16**). We also tested the replacement of the piperidine ring by a 4-hydroxymethylpiperidine, bearing a further hydrophilic function to improve water solubility, or with a cyclohexylamine moiety, thus keeping the nitrogen external to the cycle and converting it into a secondary, more basic amine (compounds **17**, **18**). Some 3-(4-nitrophenyl)-1,2,4-oxadiazole analogues bearing *N,N*-dimethylamino, *N,N*-diethylamino, or pyrrolidinomethyl chain at C5 were also prepared (compounds **19**-**21**). The influence of the length of the spacer at the C5 substituent has been evaluated by increasing it from 1 to 3 methylene groups (compare **22** and **23** with **4**). Surprisingly, when we tested the intermediate 5-(bromomethyl)- and the 5-(3-bromopropyl)-3-(4-chlorophenyl)-1,2,4-oxadiazoles **24** and **30** we noticed that they displayed more potent Sirt2 inhibition than the corresponding 5-(piperidin-1-ylmethyl) analogues **4** and **22**. Thus, we selected **30**, the most potent among them, as a new hit compound and we performed on it some structural modifications, such as the shift of the 4-chloro substituent to *meta* or *ortho* position as well as the replacement with other atoms/groups (compounds **31**-**43**). Further derivatives carrying the 3-(4-bromophenyl) moiety at C3 were prepared to gain more SAR data (compounds **44**-**46**).

Insert Figure 2

Kinetic studies and a crystal structure of Sirt2 in complex with a 1,2,4-oxadiazole analog provide mechanistic insights and interaction details for the Sirt2 inhibitory activity of our 1,2,4-oxadiazoles. Selected compounds were further tested in leukemia as well as in MDA-MB-231 breast cancer cells to determine their effects on cell cycle and apoptosis induction in cellular cancer models. Functional assays to detect the acetylation levels of α–tubulin in the NB4 leukemia cells support Sirt2 inhibition as the molecular mechanism for these compounds. Finally, two of the new 1,2,4-oxadiazole hit compounds (**35** and **39**) were tested in a large panel of leukemia cells characterized by different genotypes to determine their potential as antiproliferative agents.

## RESULTS AND DISCUSSION

**Chemistry.** The synthetic route for the preparation of the 3-aryl-1,2,4-oxadiazole derivatives **4-46** is outlined in Scheme 1. The reaction between the known *N*'-hydroxyarylimidamides **47a-m**[41-46] and the appropriate acyl halides in dry dichloromethane and in the presence of triethylamine at room temperature gave the crude *N*'-acyloxyarylimidamide intermediates that without further purification were heated in toluene or *o*-xylene at reflux to obtain the 1,2,4-oxadiazole compounds **9**, **24-43** (Scheme 1A). Compounds **4-8**, **10-23** were synthesized by treating the selected 5-(bromoalkyl)-3-(substituted)phenyl-1,2,4-oxadiazoles **24** (for **4**, **10-18**), **25** (for **5**), **26** (for **6**), **27** (for **7**), **28** (for **8**), **29** (for **19-21**), **30** (for **22**) and **33** (for **23**) with different commercially available amines, sodium iodide, and potassium carbonate in dry DMF at 60 °C for 1-2 h (Scheme 1B). The reaction of the 4-bromo-*N*'-hydroxybenzimidamide **47g** with methyl 2-chloro-2-oxoacetate or 2,2,2-trifluoroacetic anhydride in a mixture (10:1 v/v) of dry dichloromethane and dry pyridine at room

temperature or reflux directly furnished the cyclized 5-methoxycarbonyl- and 5-trifluoromethyl-1,2,4-oxadiazoles **44** and **45**, respectively. Further treatment of **44** with a 7M solution of ammonia in methanol gave the 5-carboxyamide analog **46** (Scheme 1C).

Chemical and physical data of compounds **4**-**46** are listed in Table S1 in Supporting Information.

Insert Scheme 1

**Assessment of Sirt2 inhibiting potency and selectivity.** The inhibitory effects of **4**-**24**, **30**-**46** on Sirt2 deacetylase activity were tested in a continuous assay using an α-tubulin-acetylLys40 peptide as the substrate. The residual Sirt2 activity in presence of 10 and 100 μM of the candidate inhibitors was evaluated (Figure 3A).

Insert Figure 3

Comparison of the Sirt2 inhibiting activity exerted by **4**-**8** suggests that, at the C3-phenyl ring of the 1,2,4-oxadiazole moiety, the presence as well as the position of the chlorine atom is a determinant for the inhibitory activity. Indeed, shifting it from *para* (**4**) to *meta* (**5**) position retains a certain potency, which is lost with the chlorine atom in *ortho* (**6**) or with its complete removal (**7**) or by changing the C3-phenyl to a C3-3-pyridyl ring (**8**). At the C5-methylene group of **4** it seems to be required a cyclic amine moiety for the potency against Sirt2 [see the drop of potency after its removal (**9**) or replacement with a *N*,*N*-dimethylamino group (**10**, **19**)]. Changes of the piperidine moiety of **4** with the smaller pyrrolidine (**11**), or the larger azepane (**12**) or the heteroatom-containing morpholine (**13**), thiomorpholine (**14**), piperazine (**15**, **16**), or 4-hydroxymethylpiperidine (**17**) led to compounds with similar or lower Sirt2 inhibiting potency, with

the exception of **11** and **14** that displayed higher inhibition than **4** at 100 μM. Interestingly, also the replacement of the piperidine with a cyclohexylamine moiety (**18**), thus changing a tertiary with a secondary amine function linked to the C5-methylene group, led to increased inhibition at 100 μM. Replacing the *p*-chloro with a *p*-nitro substituent at the C3-phenyl ring (**19-21**) as well as increasing the length of the spacer between the C5 oxadiazole position and the cyclic amine from 1 to 3 methylene groups (**22**, **23**), strongly decreased or totally abolished the Sirt2 inhibiting activity.

Together with these 5-aminomethyl-substituted-1,2,4-oxadiazoles, we tested also the intermediate 5-(bromomethyl)- and 5-(3-bromopropyl)-3-(4-chlorophenyl)-1,2,4-oxadiazoles **24** and **30** against Sirt2 at 10 and 100 μM. Surprisingly, they displayed a substantial improvement in potency at both tested doses with respect to the corresponding 5-(piperidin-1-ylmethyl) analogues **4** and **22** (Figure 3A). Again, shifting the chlorine atom of **30** from *para* to *meta* (**31**) or *ortho* (**32**) position as well as its total removal (**33**) decreased the Sirt2 inhibitory potency of the compounds. Replacement of the *p*-chloro with a *p*-methyl (**34**), *p*-methoxy (**35**), *p*-trifluoromethyl (**36**), *p*-nitro (**37**), *p*-fluoro (**38**), or *p*-bromo (**39**) substituent in some cases provided more potent (**34**, **37**) derivatives than **30** only at 100 μM, while with **39** the same inhibition as **30** at 10 μM and improved inhibition at 100 μM were detected. Thus a further exploration of SAR around **39** was performed, by preparing the two regioisomers **40** and **41** and by changing the C5-(3-bromopropyl) chain with a C5-(3-chloropropyl) (**42**) or a C5-(4-bromobutyl) (**43**) chain. Whilst the shift of the bromine at the C3-phenyl ring from *para* to *meta* or *ortho* position abated the Sirt2 inhibition (compare **39** with **40** and **41**), the bromo/chloro exchange at the end of the C5-side chain or its enlargement to four methylene units led to compounds still endowed with high inhibitory activity.

Finally, replacement of the 3-bromopropyl side chain at C5 of the 3-(4-bromophenyl)-1,2,4-oxadiazole scaffold with a carbomethoxy (**44**), trifluoromethyl (**45**), or carboxamide (**46**) function yielded in all cases poorly potent or inactive compounds.

In order to evaluate and compare more finely the potencies of some potent compounds we determined the $IC_{50}$ values against Sirt2 for **30**, **35-39**, **42** and **43** (Table 1). The 3-(4-bromophenyl)-5-(3-bromopropyl)-1,2,4-oxadiazole **39** was confirmed to be the most potent Sirt2 inhibitor among the synthesized oxadiazoles, it being slightly more efficient than its 3-(4-chlorophenyl) counterpart **30**. Little changes at the *para* position of the oxadiazole C3-phenyl ring (see **35-38**) or at the C5-side chain (see **42**, **43**) had only moderate effects on the Sirt2 inhibitory potency of the derivatives, with only the *p*-fluoro analog **38** being one order of magnitude less potent. We could take in account that **36**, **37**, and **43** might be slightly less potent than indicated by their $IC_{50}$ values due to an increased background, likely due to solubility limitations.

**Table 1. $IC_{50}$ Values Against Sirt2 for Selected Compounds**

| compd | structure | $IC_{50}$, μM | background, % |
|---|---|---|---|
| **30** | 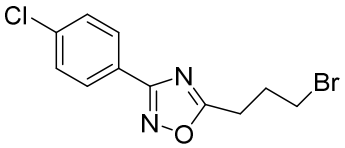 | 2.5 ± 0.2 | 12.0 |
| **35** | 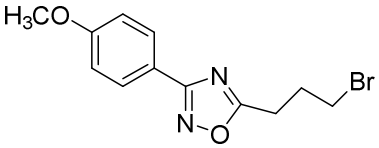 | 10.4 ± 0.2 | 19.3 |
| **36** | 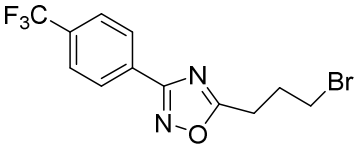 | 3.9 ± 0.3 | 32.9 |
| **37** | 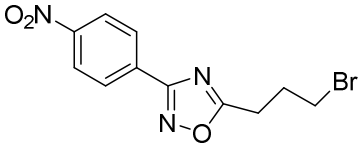 | 6.6 ± 0.9 | 27.6 |
| **38** | 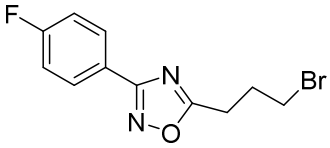 | 19.8±1.0 | 17.1 |

| | | | |
|---|---|---|---|
| **39** | 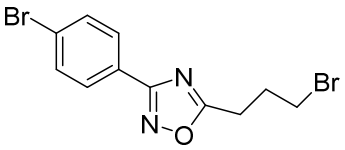 | 1.5 ± 0.1 | 15.5 |
| **42** | 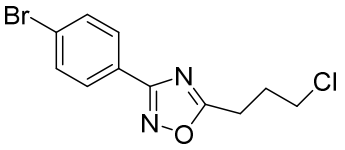 | 3.6 ± 0. 3 | 15.6 |
| **43** | 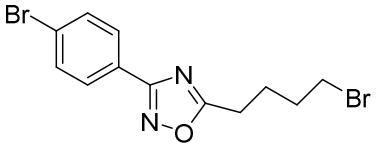 | 2.6 ± 0.4 | 25.7 |

To evaluate the isoform selectivity of the new compounds, the oxadiazoles **30**, **39** and **42** were tested against the sirtuin isoforms Sirt1, -3, and -5 (deacetylase and desuccinylase activities) using their established substrate peptides Ac-p53 (Sirt1), Ac-AceCS2 (Sirt3), and Ac-CPS1 or Suc-Prx (Sirt5), respectively (Figure 3B).

The activities of these sirtuin isoforms were not significantly affected by any of the tested 1,2,4-oxadiazole Sirt2 inhibitors at concentrations up to 100 μM. These results show that Sirt2 inhibition is not a promiscuous effect for these compounds, and that this inhibitor class displays outstanding selectivity toward Sirt2 despite its compact size. The improvement in potency and, in particular, in selectivity of the new 1,2,4-oxadiazoles compared to many known Sirt2 inhibitors is illustrated by comparison with **1**, a widely used Sirt2-specific inhibitor[28] (Figure 3B). While the inhibition of Sirt2 by **30**, **39** or **42** is slightly more pronounced than by **1**, no effect of the tested 1,2,4-oxadiazoles is seen on other Sirt isoforms at 100 μM, while **1** starts to show non-specific effects at this concentration.

**Mechanism of Sirt2 Inhibition by 1,2,4-Oxadiazoles.** To gain first insight into the inhibition mechanism of **39**, we analyzed it via Michaelis-Menten kinetic experiments. Both the α-tubulin

peptide substrate and the $NAD^+$ co-substrate were titrated at different inhibitor concentrations (Figure 4). In both cases, fitting of the individual Michaelis-Menten curves showed a decrease of $V_{max}$ and $K_m$ with increasing **39** concentrations. The complete data sets were thus fitted with an uncompetitive inhibition model, which yielded $K_m$ values of 128.5 ± 13.1 and 123.7 ± 4.2 μM, respectively for the peptide substrate and $NAD^+$. The resulting $K_i$ values of 2.2 ± 0.1 μM for **39** from both competition experiments are in good agreement with the $IC_{50}$ values (Table 1), as expected for uncompetitive inhibitors tested under substrate saturation. Comparable data were obtained from analogous competition experiments with **30** (data not shown), supporting the conclusion that this compound class inhibits uncompetitively with both substrates.

An uncompetitive mechanism, ie improved inhibition in presence of increasing substrate concentrations, indicates that the inhibitors bind to a closed conformation of Sirt2 induced by substrate binding.

Insert Figure 4

**Crystal Structure of Sirt2 in Complex with a 1,2,4-Oxadiazole Analog and ADP-ribose.** To characterize further the inhibition mechanism and binding details of our compounds, we tried a variety of co-crystallization and soaking approaches for solving a complex structure. Finally, we were able to solve the structure of a Sirt2/1,2,4-oxadiazole complex by soaking the compound **30** in Sirt2/ADP-ribose crystals. The resulting high-resolution structure was refined to $R_{cryst}/R_{free}$ values of 17.3/19.4 % (Table 2) and contained well defined electron density for both the ADP-ribose molecule and for the 1,2,4-oxadiazole inhibitor (Figure 5A and Figure S2 in Supporting Information). The electron density located in the hydrophobic pocket at the back of the active site of Sirt2 can clearly be attributed to the soaked ligand, however the abnormally high B-factors for the

Br atom as well as the presence of significant residual negative density in the Fourier difference map after refinement (Figure S3 in Supporting Information) led to the conclusion that rather than compound **30**, an analogue of this compound with a hydroxyl group instead of the bromine at the C5 substituent, the 5-(3-hydroxypropyl)-3-(4-chlorophenyl)-1,2,4-oxadiazole **48**, is bound to Sirt2 (Figure S3). This observation is further supported by the absence of any anomalous signal for a Br atom in this region although the data were collected at the bromine K absorption edge. Hydrolysis of bromoalkyl chains in water and/or buffer has been reported before,[47-48] and the sonication, heating, and freeze-thawing pre-treatment employed for the crystal soaking experiments appear to have amplified the bromo-hydroxy exchange (Figure S4 in Supporting information). Surprisingly, all attempts to crystallize pure **30** and **39** with Sirt2 and ADP-ribose were unsuccessful leading to more than 20 empty crystal structures, and only when the bromo-hydroxy conversion of **30** to **48** in part occurred (Figure S4) we were able to obtain a complex.

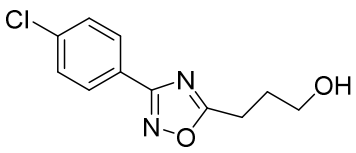


**48**

**Table 2. Diffraction Data and Refinement Statistics**

| | Sirt2/ADP-ribose/48 complex |
|---|---|
| **Diffraction Data Statistics** | |
| Wavelength (Å) | 0.9184 |
| Resolution range (Å) | 48.93-1.89 (1.93-1.89) |
| Space group | $P2_12_12_1$ |
| Unit cell (Å) | 76.56 76.71 113.83 |
| Total reflections | 399403 (24802) |
| Unique reflections | 54438 (3465) |
| Completeness (%) | 100 (100) |
| Multiplicity | 7.3 (7.2) |
| Mean I/σ(I) | 14.4 (2.5) |
| Wilson B-factor | 26.3 |
| R-merge (%) | 9.0 (74.1) |
| R-meas (%) | 10.4 (86.8) |
| CC1/2 (%) | 99.9 (56.0) |
| | |
| **Refinement Statistics** | |
| R-work (%) | 17.3 (28.1) |
| R-free (%) | 19.4 (28.7) |
| Non H atoms | 5494 |
| Protein | 4840 |
| Ligands (Zn, **48**, ADP-ribose) | 106 |
| Solvent | 476 |
| RMSD(bonds) (Å) | 0.003 |
| RMSD(angles) (°) | 0.66 |
| Ramachandran most favored (%) | 97 |
| Ramachandran outliers (%) | 0.16 |
| Average B-factor (Å²) | 38.2 |
| Protein (Å²) | 37.3 |
| Ligands (Å²) (Zn, ADPr, **48**) | 34.0 |
| Solvent (Å²) | 45.3 |

Insert Figure 5

To analyze the capability of **48** to inhibit Sirt2, we synthesized and tested it in our enzyme assay (see Scheme S1 and Figure S5 in Supporting Information). The obtained $IC_{50}$ values against Sirt2 for **48** and its acetyl analog **49**, intermediate for the synthesis, are: 41.2 ± 11.9 μM for **48**, and 21.2 ± 3.8 μM for **49**. These results confirm that **48** is still active against Sirt2, but less potent than **30**, and that the insertion of a highly polar substituent (ie, hydroxyl) at the C5 chain causes a severe drop of Sirt2 inhibition. However, such loss of potency can be in part counteracted by converting the hydroxyl into an acetoxy function (**48** to **49**). Thus, the hydroxyl group of **48** enables inhibition and crystal structure analysis of the Sirt2 complex with this compound family representative, but it is not required for highly potent inhibition.

The conversion from **30** to **48** also raises the possibility of a covalent mode of inhibition, however such a mechanism is very unlikely. First, no covalent connection can be observed in the crystal structure between **48** and either Sirt2 or ADP-ribose (Figure S2 in Supporting Information; see below). In addition, preincubation of Sirt2 with **39** (or **30**) did not reveal any influence on the compound inhibitory potency, which further support the fact that inhibition mechanism of this compound family does not involve covalent modification of the enzyme (Figure S6 in Supporting Information).

In the Sirt2/**48** complex, the compound occupies the acyl channel at the back of the active site of Sirt2 with its alkyl chain positioned in the extended C-site ("ECS-I" in reff.[49-50]) and its *para*-chloro phenyl located in a sub-cavity of the large hydrophobic pocket (see below). The ligand is stabilized by hydrogen bonds of the 5-hydroxyl of **48** to the main-chain carbonyl atom of Val233 and to the 2'-hydroxyl atom of ADP-ribose. However, these interactions are not essential for potent inhibition, since **30** with its bromine inhibits Sirt2 much more potently (>10-fold) than **48**. All other

interactions are van der Waals interactions and involve the side chains of Phe96 and 119, of Leu134, 138 and 297, of Ile169 and 232 (Figure 5B and Figure S7 in Supporting Information). As already observed in other Sirt2 crystal structures, the electron density for the loop residues 139-141 is relatively weak, and the exact position of the side chain of Leu138, notably, is uncertain indicating that although **48** binds at the proximity of this flexible region, it does not seem to stabilize its conformation. The C-site, which is dedicated to bind the carboxamide group of nicotinamide, is not covered by **48** and instead occupied by a molecule of DMSO (Figure 5A and 5B).

The overall Sirt2 conformation in the Sirt2/**48** complex is similar to that in the original, unsoaked crystal structure. Indeed, superposition of the crystal structures of Sirt2 in complex with ADP ribose to our ligand complex yields low rmsd values [3zgv (0.36 Å) and 5d7o (0.79 Å) on 300 $C_\alpha$ positions] and thus indicate that binding of the ligand does not induce any major conformational rearrangement (Figure 5C). Most of the differences are located in two regions; the 135-142 flexible loop which connects the zinc-binding and Rossmann-fold domains and constitute part of the ligand binding site and the α-helix 205-217 which forms interactions with the former loop.

Comparing the Sirt2/**48** complex to other Sirt2 inhibitor structures shows that the overall protein conformation is very similar to the one observed for complexes with the (*S)*-6-chloro-2,3,4,9-tetrahydro-1*H*-carbazole-1-carboxamide Ex-243 (**50**)[51] (the *S* enantiomer of the 6-chloro-2,3,4,9-tetrahydro-1*H*-carbazole-1-carboxamide Ex-527 (**51**)[52]) and its derivative CHIC35 [(*S*)-2-chloro-5,6,7,8,9,10-hexahydro-cyclohept[b]indole-6-carboxamide][51] (rmsd on 301 and 302 $C_\alpha$ positions of 0.43 Å and 0.39 Å respectively with PDB: 5d7p and 5d7q). This finding is consistent with the fact that **48** as well as **50** occupy the extended C-site in presence of a nucleotide co-ligand and that both complex structures were in fact obtained using the same target conformation through soaking of a Sirt2/ADP-ribose complex. In contrast, superposition of Sirt2/**48** with the complex of Sirt2 with **2**[31] and $NAD^+$ (PDBid: 4rmg) yields an rmsd of 2.0 Å. Most conformational differences between these

two structures are due to the fact that **2** blocks Sirt2 in a so called "blocked-open" conformation, in which the zinc-binding domain is not fully closing the active site (Figure 5D). It is interesting to note that our compound, which is smaller than **2**, is able to bind to the closed conformation of Sirt2, which is also in agreement with the fact that the 1,2,4-oxadiazoles described here are uncompetitive inhibitors and therefore bind to an "active" conformation of the protein.

As illustrated by a superposition of representative Sirt2 inhibitors (Figure 6A), the 1,2,4-oxadiazole **48** exhibits an unprecedented orientation in the large, hydrophobic acyl channel pocket thereby addressing another, Sirt2-specific sub cavity by intercalating between the side chains of Leu134 and Leu138. This cavity, uniquely occupied by our compounds, might explain their exceptional Sirt2-selectivity and can be exploited in further Sirt2 inhibitor development based on our and also other scaffolds. The superposition of our Sirt2 complex structure with that of the inhibitory macrocyclic peptide **3**[39] (Figure 6A; PDBid 4l3o) indicates that the conformation of the 1,2,4-oxadiazole is incompatible with the presence of an acetyl substrate peptide as the two molecules are clashing. It is, however, conceivable that in the inhibitory relevant quaternary complex between Sirt2, substrate, co-substrate, and 1,2,4-oxadiazole, slight conformational changes allows the 1,2,4-oxadiazole inhibitor to stale catalysis, or that inhibitor binding in fact takes place after intermediate or even product formation, as observed with **50**/**51**.[49]

To compare our complex structure with the SAR data, a set of 1,2,4-oxadiazoles were modelled inside the active site of Sirt2 based on the crystal structure (Figure 6B-E). As exemplified by the model with **4**, the active site of Sirt2 cannot accommodate too bulky groups at the C5 position of the 1,2,4-oxadiazole ring (Figure 6C). The SAR results about the substitution at the C3 phenyl ring are also supported by the model of **40** and **41**, because the shift of the chlorine atom from *para* to either *meta* or *ortho* position at the phenyl ring introduce deleterious steric hindrance in the binding pocket (Figures 6D and 6E).

Insert Figure 6

**1,2,4-Oxadiazoles on Cancer Cells.** The 1,2,4-oxadiazoles **4-24**, **30-46** were tested in U937 human leukemia cells at 25 μM for 48 h to determine their effects on cell cycle and induction of apoptosis (Figure 7). Under the tested conditions, the majority of the compounds did not alter the percentage of cell cycle phases with respect to the control. The only exceptions were compounds **24**, **32** and **41**, which blocked cell cycle at the G2/M phase, and **35**, which gave arrest at the S phase (Figure 7A). The same compounds, including also **38**, displayed the highest apoptosis induction, determined as fraction of cells in pre-G1 peak, with percentages in the range 11.1-37.1%.

Insert Figure 7

Compounds **30**, **35**, **38** and **39** were chosen according to their potency in Sirt2 inhibition and/or apoptosis induction in U937 cells, and were tested against a panel of leukemia cells (U937, NB4, HL-60, and K562) as well as against breast cancer MDA-MB-231 cells for 48 h at 5, 10, 25 and 50 μM. The relative dose-response curves for apoptosis induction (pre-G1 peak percentage) are depicted in Figure 8A: among the tested compounds, **39** was highly potent against NB4 cells already at 10 μM, and displayed >80% of apoptosis in U937 cells at 50 μM. Compound **35** was the most efficient (>80%) as apoptosis inducer at 25 μM in 3 out of 5 cell lines (NB4, K562 and MDA-MB-231), while **38** showed 30-40% apoptosis only at 50 μM against NB4 and MDA-MB-231 cells, and **30** was in general less effective. In the same assays, **1** was totally unable to elicit apoptosis, giving only 6% apoptosis in HL-60 cells at the highest tested dose (Figure S8 in Supporting Information).

Insert Figure 8

To confirm that our 1,2,4-oxadiazoles worked in the tested cells by inhibiting Sirt2, the levels of acetyl-α-tubulin were detected in NB4 and in U937 cells treated with **35** and **39** (5 and 25 μM) for 4 (NB4) or 24 (U937) h (Figure 8B). Compound **1** was used as a reference drug, and the suberoylanilide hydroxamic acid (SAHA, **52**) as a positive control. Western blot analyses in both cell lines showed no substantial effect on acetyl-α-tubulin levels by **1**, while **35** and **39** increased α–tubulin acetylation.

Compounds **35** and **39** were further tested in a large panel of leukemia cells characterized by different genotypes (OCI-AML3, IMS-M2, OCI-AML2, MV4-11, Kasumi-1, Karpass299) in addition to the already used U937, HL-60 and NB4, to determine their antiproliferative effects. The relative $IC_{50}$ values are listed in Table 3. Among the tested cell lines, **35** arrested the growth of Kasumi-1 and NB4 cells at its biochemical $IC_{50}$ value (10 μM), and that of MV4-11 and IMS-M2 cells at slightly higher concentration, while with OCI-AML3 showed the lowest efficacy. Instead, **39** showed a general reduced antiproliferative effect compared to **35**, with a preferential efficacy against Karpass299, MV4-11 and NB4 cell lines.

**Table 3. Antiproliferative Effect ($IC_{50}$ values) Displayed by 35 and 39 in a Panel of Leukemia Cell Lines**

| cell line | sub-type | alterations | $IC_{50}$, μM | |
|---|---|---|---|---|
| | | | **35** | **39** |
| OCI-AML3 | AML[a] | $NPM1c^{+}$, DNMT3A (R882C) | 62 ± 6 | 66 ± 2 |

| | | | | |
|---|---|---|---|---|
| IMS-M2 | AML | NPM1c$^{+}$, no other informations | 18.4 ± 0.4 | 100 ± 1 |
| OCI-AML2 | AML | DNMT3A (R635W) | 37 ± 2 | 85 ± 5 |
| MV4-11 | AML | FLT3-ITD, [t(4;11)(q21;q23)], MLL/MLLT2(AF4) | 16 ± 2 | 38 ± 8 |
| Kasumi-1 | AML | AML1-ETO [t(8:21)] | 10.3 ± 0.3 | 56 ± 3 |
| U937 | AML | p53$^{+/-}$ | 25 ± 5 | >100 |
| NB4 | APL[b] | PML-RARα, [t(15;17)(q22;q12)] | 12 ± 2 | 49 ± 1 |
| HL-60 | APL | p53$^{-/-}$ | 30 ± 3 | 100 ± 2 |
| Karpass299 | ALCL[c] | NPM1/ALK, [t(2;5)(p23;q35)] | 36 ± 3 | 25 ± 6 |

[a]AML, Acute Myeloid Leukemia. [b]APL, Acute Promyelocytic Leukemia. [c]ALCL, Anaplastic Large Cell Lymphoma.

## CONCLUSION

Among the epigenetic players (writers, readers and erasers), the class III deacetylase Sirt2 is widely recognized as an attractive target for treatment of neurodegenerative disorders,[11] metabolic dysfunctions,[53] age-related diseases,[10] and cancer,[9, 54] although its role in the last disease is still debated.[25, 55] A number of Sirt2 inhibitors have been reported to date,[23, 28-29, 31-39] but they suffer from scarce Sirt2 isoform selectivity and/or they have been studied in CNS rather than in cancer contexts. Here we describe the identification of a new series of Sirt2 inhibitors, based on the 1,2,4-oxadiazole scaffold, starting from the hit compound 3-(4-chlorophenyl)-5-(piperidin-1-ylmethyl)-1,2,4-oxadiazole **4** previously disclosed by us through virtual screening procedures.[40] Extensive SAR studies applied on this compound by using the α-tubulin-acetylLys40 peptide as the Sirt2 substrate highlighted the presence of a *para*-substituted phenyl ring at the C3 position and of a cyclic aminomethyl or a ω–haloalkyl chain at the C5 position of the 1,2,4-oxadiazole scaffold as

crucial determinants to gain Sirt2 inhibition. Selected compounds showed $IC_{50}$ values in the low, single-digit μM range, and were inactive up to 100 μM against Sirt1, Sirt3 and Sirt5 (deacetylase and desuccinylase activities). Mechanistic studies performed on the C3-*para*-bromophenyl **39** showed uncompetitive inhibition with respect to both the α–tubulin peptide substrate and the $NAD^+$ co-substrate, and the crystal structure of Sirt2 in complex with the 3-(4-chlorophenyl)-5-(3-hydroxypropyl)-1,2,4-oxadiazole **48** and ADP-ribose was determined. The superposition of the complex structure between Sirt2 and **48** with that of some representative Sirt2 inhibitor complexes revealed that **48** exhibits an unprecedented orientation in the large hydrophobic pocket addressing another sub cavity by intercalating between the side chains of Leu134 and Leu138, a cavity never exploited before that may constitute a rationale for further Sirt2 inhibitor development, also starting from other scaffolds. Development of more potent inhibitors based on our 1,2,4-oxadiazole moiety could be pursued by further extension of the 3-(4-chlorophenyl) substituent to address either the Sirt2 'selectivity pocket' occupied by the SirReal inhibitors or by introducing interactions within the C-site, taking over the position of the DMSO molecule bound in our Sirt2/**48** complex structure.

When tested in human leukemia (U937, NB4, HL-60 and K562) cell lines as well as against the breast cancer MDA-MB-231 cell lines, **35** gave >80% of apoptosis at 25 μM in NB4, K562 and MDA-MB-231 cell lines, and **39** was able to induce the same effect in NB4 cells already at 10 μM. These compounds, when analyzed in Western blot assay to detect their effects on the acetyl-α-tubulin levels in NB4 cells, displayed an increase of α-tubulin acetylation confirming the involvement of Sirt2 inhibition in their activity. Compound **1**, tested at the same condition, was practically inactive in both apoptosis induction assays and Western blot analysis.

AML is a disease that groups heterogeneous hematopoietic stem cell disorders. Several recurrent chromosomal alterations are involved in AML pathogenesis, such as aberrant fusion proteins AML1-ETO, PML-RARα or mutant proteins as $NPM1c^+$, FLT3-ITD or DNMT3A. Thus, we tested

**35** and **39** against a panel of leukemia cell lines characterized by different alterations. The $IC_{50}$ values reported in Table 3 show that **35** was able to reduce 50% cell growth in Kasumi-1 and NB4 cell lines at its $IC_{50}$ biochemical value as Sirt2 inhibitor (10 μM), and in MV4-11 and IMS-M2 cell lines at concentration slightly higher, while **39** showed reduced potency and a preferential efficacy against Karpass299, MV4-11 and NB4 cell lines. Further studies will be performed on this 1,2,4-oxadiazole series of Sirt2 inhibitors to improve their potency and their anticancer potential.

## EXPERIMENTAL SECTION

**Chemistry**. Melting points were determined on a Stuart melting point apparatus SMP10. $^1$H-NMR spectra were recorded at 400 MHz using a Bruker AC 400 spectrometer; chemical shifts are reported in δ (ppm) units relative to the internal reference tetramethylsilane ($Me_4Si$). Mass spectra were recorded on an API-TOF Mariner by Perspective Biosystem (Stratford, TX, USA), and samples were injected by an Harvard pump using a flow rate of 5-10 μL/min, infused in the Electrospray system. All compounds were routinely checked by TLC and $^1$H-NMR. TLC was performed on aluminum-backed silica gel plates (Merck DC, Alufolien Kieselgel 60 $F_{254}$) with spots visualized by UV light or using a $KMnO_4$ alkaline solution. All solvents were reagent grade and, when necessary, were purified and dried by standard methods. Concentration of solutions after reactions and extractions involved the use of a rotary evaporator operating at reduced pressure of ~ 20 Torr. Organic solutions were dried over anhydrous sodium sulfate. Elemental analysis has been used to determine purity of the described compounds, that is >95%. Analytical results are within ± 0.40% of the theoretical values (Table S2 in Supporting Information). All chemicals were purchased from Sigma Aldrich s.r.l., Milan (Italy) or from TCI Europe N.V., Zwijndrecht (Belgium), and were of the highest purity. As a rule, samples prepared for physical and biological

studies were dried in high vacuum over $P_2O_5$ for 20 h at temperatures ranging from 25 to 40 °C, depending on the sample melting point.

General procedures for the syntheses of the 1,2,4-oxadiazoles **9**, **24-43** (General Procedure A) and of **4-8**, **10-23** (General Procedure B), spectral data for the final compounds **4-24**, **30-43**, and syntheses and spectral data of compounds **44-46** are described below. Syntheses and spectral data of compounds **48** and **49** as well as chemical and physical data of compounds **4-46**, **48** and **49** are reported in Supporting Information.

**General Procedure for the Preparation of the 1,2,4-Oxadiazoles 9, 24-43 (General Procedure A).** A solution of the appropriate (ω–halo)acyl chloride (1.32 mmol) in dry dichloromethane (2 mL) was added dropwise, while cooling at 0 °C, to a solution of the proper (*Z*)-*N*'-hydroxybenzimidamide **47** (0.88 mmol) in dry dichloromethane (3 mL) in the presence of triethylamine (1.58 mmol). The reaction mixture was stirred at 0 °C for 10 min and then at room temperature for 2 h. After the completion of the reaction, the mixture was evaporated at reduced pressure and the resulting crude product was triturated with water (10 mL) for 1 h and then filtered to afford the related (*Z*)-*N*'-[(ω-haloacyl)oxy]benzimidamide as a pink solid that was used in the next step without further purification.

The crude (*Z*)-*N*'-[(ω-haloacyl)oxy]benzimidamide (0.852 mmol) was dissolved in dry toluene (10 mL) and stirred at reflux for 5 h. Toluene was then evaporated under reduced pressure at 60 °C to achieve a brown/orange crude product that was purified by a silica gel column eluting with a mixture ethyl acetate:*n*-hexane 1:30 to give the final product.

**General Procedure for the Preparation of the 1,2,4-Oxadiazoles 4-8, 10-23 (General Procedure B).** A mixture of 5-(bromoalkyl)-3-aryl)-1,2,4-oxadiazole (among **24-30** or **33**) (0.365 mmol), piperidine (1.82 mmol), sodium iodide (0.402 mmol) and dry potassium carbonate (0.548 mmol) in dry DMF (1.5 mL) was heated while stirring at 60 °C for 1 h. The reaction was then

allowed to cool to room temperature, quenched with water (18 mL) and extracted with ethyl acetate (4 × 25 mL). The combined organic phases were washed with brine, dried over sodium sulfate, filtered and evaporated under vacuum to afford a residue that was purified by a silica gel column eluting with a mixture ethyl acetate:*n*-hexane 1:5 to give the pure final product.

**3-(4-Chlorophenyl)-5-(piperidin-1-ylmethyl)-1,2,4-oxadiazole (4) (General Procedure B).** $^1$H-NMR (400 MHz; $CDCl_3$) δ 1.44-1.50 (m, 2H, C*H*$_2$ piperidine ring), 1.64-1.69 (m, 4H, 2 × C*H*$_2$ piperidine ring), 2.59-2.61 (m, 4H, 2 × C*H*$_2$ piperidine ring), 3.90 (s, 2H, oxadiazole-C*H*$_2$N), 7.47-7.49 (d, *J* = 8.8 Hz, 2H, C*H* benzene ring), 8.05-8.08 (d, *J* = 8.8 Hz, 2H, C*H* benzene ring). MS (ESI), m/z: 278 $[M + H]^+$.

**3-(3-Chlorophenyl)-5-(piperidin-1-ylmethyl)-1,2,4-oxadiazole (5) (General Procedure B).** $^1$H-NMR (400 MHz; $CDCl_3$) δ 1.45-1.50 (m, 2H, C*H*$_2$ piperidine ring), 1.62-1.70 (m, 4H, 2 × C*H*$_2$ piperidine ring), 2.58-2.61 (t, 4H, 2 × C*H*$_2$ piperidine ring), 3.91 (s, 2H, oxadiazole-C*H*$_2$N), 7.42-7.51 (m, 2H, C*H* benzene ring), 8.00-8.02 (m, 1H, C*H* benzene ring), 8.14 (s, 1H, C*H* benzene ring). MS (ESI), m/z: 278 $[M + H]^+$.

**3-(2-Chlorophenyl)-5-(piperidin-1-ylmethyl)-1,2,4-oxadiazole (6) (General Procedure B).** $^1$H-NMR (400 MHz; $CDCl_3$) δ 1.45-1.49 (m, 2H, C*H*$_2$ piperidine ring), 1.63-1.69 (m, 4H, 2 × C*H*$_2$ piperidine ring), 2.58-2.61 (m, 4H, 2 × C*H*$_2$ piperidine ring), 3.95 (s, 2H, oxadiazole-C*H*$_2$N), 7.38-7.47 (m, 2H, C*H* benzene ring), 7.55-7.57 (m, 1H, C*H* benzene ring), 7.95-7.97 (m, 1H, C*H* benzene ring). MS (ESI), m/z: 278 $[M + H]^+$.

**3-Phenyl-5-(piperidin-1-ylmethyl)-1,2,4-oxadiazole (7) (General Procedure B).** $^1$H-NMR (400 MHz; $CDCl_3$) δ 1.46-1.48 (m, 2H, C*H*$_2$ piperidine ring), 1.65-1.68 (m, 4H, 2 × C*H*$_2$ piperidine ring), 2.60 (m, 4H, 2 × C*H*$_2$ piperidine ring), 3.91 (s, 2H, oxadiazole-C*H*$_2$N), 7.50-7.51 (m, 3H, C*H* benzene ring), 8.11-8.14 (m, 2H, C*H* benzene ring). MS (ESI), m/z: 244 $[M + H]^+$.

**5-(Piperidin-1-ylmethyl)-3-(pyridin-3-yl)-1,2,4-oxadiazole (8) (General Procedure B).** $^1$H-

NMR (400 MHz; $CDCl_3$) δ 1.43-1.48 (m, 2H, C*H*$_2$ piperidine ring), 1.54-1.68 (m, 4H, 2 × C*H*$_2$ piperidine ring), 2.60 (t, 4H, 2 × C*H*$_2$ piperidine ring), 3.93 (s, 2H, oxadiazole-C*H*$_2$N), 7.43-7.46 (m, 1H, C*H* pyridine ring), 8.39-8.41 (m, 1H, C*H* pyridine ring), 8.76-8.77 (m, 1H, C*H* pyridine ring), 9.35 (s, 1H, C*H* pyridine ring). MS (ESI), m/z: 245 $[M + H]^+$.

**3-(4-Chlorophenyl)-5-methyl-1,2,4-oxadiazole (9) (General Procedure A).** $^1$H-NMR (400 MHz; $CDCl_3$) δ 2.68 (s, 3H, C*H*$_3$), 7.47-7.49 (d, *J* = 8.4 Hz, 2H, C*H* benzene ring), 8.01-8.03 (d, *J* = 8.4 Hz, 2H, C*H* benzene ring). MS (ESI), m/z: 195 $[M + H]^+$.

**1-(3-(4-Chlorophenyl)-1,2,4-oxadiazol-5-yl)-*N*,*N*-dimethylmethanamine (10) (General Procedure B).** $^1$H-NMR (400 MHz; $CDCl_3$) δ 2.45 (s, 6H, 2 × C*H*$_3$), 3.88 (s, 2H, oxadiazole-C*H*$_2$N), 7.47-7.49 (d, *J* = 8.4 Hz, 2H, C*H* benzene ring), 8.06-8.08 (d, *J* = 8.4 Hz, 2H, CH benzene ring). MS (ESI), m/z: 238 $[M + H]^+$.

**3-(4-Chlorophenyl)-5-(pyrrolidin-1-ylmethyl)-1,2,4-oxadiazole (11) (General Procedure B).** $^1$H-NMR (400 MHz; $CDCl_3$) δ 1.95-1.99 (m, 4H, 2 × C*H*$_2$ pyrrolidine ring), 2.83-2.92 (m, 4H, 2 × C*H*$_2$ pyrrolidine ring), 4.03 (s, 2H, oxadiazole-C*H*$_2$N), 7.46-7.48 (d, *J* = 8.4 Hz, 2H, C*H* benzene ring), 8.06-8.08 (d, *J* = 8.4 Hz, 2H, C*H* benzene ring). MS (ESI), m/z: 263 $[M + H]^+$.

**5-(Azepan-1-ylmethyl)-3-(4-chlorophenyl)-1,2,4-oxadiazole (12) (General Procedure B).** $^1$H-NMR (400 MHz; $CDCl_3$) δ 1.62-1.63 (m, 4H, 2 × C*H*$_2$ azepane ring), 1.71 (m, 4H, 2 × C*H*$_2$ azepane ring), 2.82-2.85 (m, 4H, 2 × C*H*$_2$ azepane ring), 4.07 (s, 2H, oxadiazole-C*H*$_2$N), 7.46-7.49 (d, *J* = 8.4 Hz, 2H, C*H* benzene ring), 8.05-8.07 (d, *J* = 8.4 Hz, 2H, C*H* benzene ring). MS (ESI), m/z: 292 $[M + H]^+$.

**4-((3-(4-Chlorophenyl)-1,2,4-oxadiazol-5-yl)methyl)morpholine (13) (General Procedure B).** $^1$H-NMR (400 MHz; $CDCl_3$) δ 2.68-2.70 (m, 4H, 2 × C*H*$_2$ morpholine ring), 3.78-3.80 (t, 4H, 2 × C*H*$_2$ morpholine ring), 3.93 (s, 2H, oxadiazole-C*H*$_2$N), 7.47-7.49 (d, *J* = 8.4 Hz, 2H, C*H* benzene ring), 8.05-8.07 (d, *J* = 8.4 Hz, 2H, C*H* benzene ring). MS (ESI), m/z: 280 $[M + H]^+$.

**3-(4-Chlorophenyl)-5-(thiomorpholinomethyl)-1,2,4-oxadiazole (14) (General Procedure B).** $^1$H-NMR (400 MHz; $CDCl_3$) δ 2.74-2.77 (t, 4H, 2 × C$H_2$ thiomorpholine ring), 2.92-2.95 (m, 4H, 2 × C$H_2$ thiomorpholine ring), 3.95 (s, 2H, oxadiazole-C$H_2$N), 7.47-7.49 (d, $J$ = 8.4 Hz, 2H, C*H* benzene ring), 8.05-8.07 (d, $J$ = 8.4 Hz, 2H, C*H* benzene ring). MS (ESI), m/z: 296 $[M + H]^+$.

**3-(4-chlorophenyl)-5-((4-methylpiperazin-1-yl)methyl)-1,2,4-oxadiazole (15) (General Procedure B).** $^1$H-NMR (400 MHz; $CDCl_3$) δ 2.32 (s, 3H, C$H_3$), 2.45-2.62 (m, 4H, 2 × C$H_2$ piperazine ring), 2.64-2.80 (m, 4H, 2 × C$H_2$ piperazine ring), 3.94 (s, 2H, oxadiazole-C$H_2$N), 7.47-7.49 (d, $J$ = 8.0 Hz, 2H, C*H* benzene ring), 8.04-8.06 (d, $J$ = 8.0 Hz, 2H, C*H* benzene ring). MS (ESI), m/z: 293 $[M + H]^+$.

**3-(4-Chlorophenyl)-5-((4-phenylpiperazin-1-yl)methyl)-1,2,4-oxadiazole (16) (General Procedure B).** $^1$H-NMR (400 MHz; $CDCl_3$) δ 2.84-2.87 (m, 4H, 2 × C$H_2$ piperazine ring), 3.28-3.30 (m, 4H, 2 × C$H_2$ piperazine ring), 4.01 (s, 2H, oxadiazole-C$H_2$N), 6.87-6.88 (m, 1H, C*H* benzene ring), 6.91-6.96 (d, 2H, C*H* benzene ring), 7.28-7.31 (m, 2H, C*H* benzene ring), 7.48-7.50 (d, $J$ = 8.4 Hz, 2H, C*H* benzene ring), 8.06-8.08 (d, $J$ = 8.4 Hz, 2H, C*H* benzene ring). MS (ESI), m/z: 355 $[M + H]^+$.

**(1-((3-(4-Chlorophenyl)-1,2,4-oxadiazol-5-yl)methyl)piperidin-4-yl)methanol (17) (General Procedure B).** $^1$H-NMR (400 MHz; $CDCl_3$) δ 1.29-1.44 (m, 3H, C*H*$CH_2$OH and 2 × CH*H* piperidine ring), 1.78-1.81 (d, 2H, 2 × CH*H* piperidine ring), 2.24-2.29 (t, 2H, 2 × CH*H* piperidine ring), 3.04-3.07 (d, 2H, 2 × CH*H* piperidine ring), 3.52-3.54 (m, 2H, C$H_2$OH), 3.93 (s, 2H, oxadiazole-C$H_2$N), 7.47-7.49 (d, $J$ = 8.4 Hz, 2H, C*H* benzene ring), 8.05-8.07 (d, $J$ = 8.4 Hz, 2H, C*H* benzene ring). MS (ESI), m/z: 308 $[M + H]^+$.

***N*-((3-(4-Chlorophenyl)-1,2,4-oxadiazol-5-yl)methyl)cyclohexanamine (18) (General Procedure B).** $^1$H-NMR (400 MHz; $CDCl_3$) δ 1.14-1.29 (m, 4H, 2 × C$H_2$ cyclohexane ring), 1.63-1.78 (m, 4H, 2 × C$H_2$ cyclohexane ring), 1.92-1.95 (d, 2H, 2 × CH*H* cyclohexane ring), 2.52-2.56

(m, 1H, $CH_2CHCH_2$ cyclohexane ring), 4.16 (s, 2H, oxadiazole-$CH_2NH$), 7.47-7.49 (d, $J$ = 8.8 Hz, 2H, C*H* benzene ring), 8.04-8.06 (d, $J$ = 8.8 Hz, 2H, C*H* benzene ring). MS (ESI), m/z: 292 $[M + H]^+$.

***N*,*N*-Dimethyl-1-(3-(4-nitrophenyl)-1,2,4-oxadiazol-5-yl)methanamine (19) (General Procedure B).** $^1$H-NMR (400 MHz; $CDCl_3$) δ 2.46 (s, 6H, 2 × $CH_3$), 3.91 (s, 2H, oxadiazole-$CH_2N$), 8.32-8.38 (m, 4H, C*H* benzene ring). MS (ESI), m/z: 249 $[M + H]^+$.

***N*-Ethyl-*N*-((3-(4-nitrophenyl)-1,2,4-oxadiazol-5-yl)methyl)ethanamine (20) (General Procedure B).** $^1$H-NMR (400 MHz; $CDCl_3$) δ 1.15-1.18 (t, $J$ = 7.2 Hz, 6H, 2 × $CH_2CH_3$), 2.68-2.74 (q, $J$ = 7.2 Hz, 4H, 2 × $CH_2CH_3$), 4.07 (s, 2H, oxadiazole-$CH_2N$), 8.31-8.38 (m, 4H, C*H* benzene ring). MS (ESI), m/z: 277 $[M + H]^+$.

**3-(4-Nitrophenyl)-5-(pyrrolidin-1-ylmethyl)-1,2,4-oxadiazole (21) (General Procedure B).** $^1$H-NMR (400 MHz; $CDCl_3$) δ 1.90-1.94 (m, 4H, 2 × $CH_2$ pyrrolidine ring), 2.74-2.77 (m, 4H, 2 × $CH_2$ pyrrolidine ring), 4.07 (s, 2H, oxadiazole-$CH_2N$), 8.32-8.38 (m, 4H, C*H* benzene ring). MS (ESI), m/z: 275 $[M + H]^+$.

**3-(4-Chlorophenyl)-5-(3-(piperidin-1-yl)propyl)-1,2,4-oxadiazole (22) (General Procedure B).** $^1$H-NMR (400 MHz; $CDCl_3$) δ 1.42-1.43 (m, 2H, $CH_2$ piperidine ring), 1.52-1.57 (m, 4H, $CH_2$ piperidine ring), 2.03-2.10 (m, 2H, $CH_2CH_2CH_2N$), 2.38-2.44 (m, 6H, 2 × $CH_2$ piperidine ring and CH2CH2C$H_2$N), 2.98-3.01 (t, $J$ = 7.2 Hz, 2H, $CH_2CH_2CH_2N$), 7.46-7.48 (d, $J$ = 8.4 Hz, 2H, C*H* benzene ring), 8.02-8.04 (d, $J$ = 8.4 Hz, 2H, C*H* benzene ring). MS (ESI), m/z: 306 $[M + H]^+$.

**2-(4-(3-(3-Phenyl-1,2,4-oxadiazol-5-yl)propyl)piperazin-1-yl)ethan-1-ol (23) (General Procedure B).** $^1$H-NMR (400 MHz; $CDCl_3$) δ 1.75 (m, 2H, $CH_2CH_2CH_2N$ ), 2.04-2.11 (m, 2H, $CH_2CH_2CH_2N$), 3.28-3.30 (m, 10H, 4 × $CH_2$ piperazine ring and $CH_2CH_2CH_2N$), 3.00-3.04 (t, $J$ = 7.2 Hz, 2H, $CH_2CH_2OH$), 3.59-3.62 (t, $J$ = 5.2 Hz, 2H, $CH_2CH_2OH$), 7.49-7.51 (m, 3H, C*H* benzene ring), 8.07-8.10 (m, 2H, C*H* benzene ring). MS (ESI), m/z: 317 $[M + H]^+$.

**5-(Bromomethyl)-3-(4-chlorophenyl)-1,2,4-oxadiazole (24) (General Procedure A).** $^1$H-NMR (400 MHz; $CDCl_3$) δ 4.57 (s, 2H, C*H*$_2$Br), 7.48-7.50 (d, *J* = 8.4 Hz, 2H, C*H* benzene ring), 8.03-8.05 (d, *J* = 8.4 Hz, 2H, C*H* benzene ring). MS (ESI), m/z: 273 $[M + H]^+$.

**5-(3-Bromopropyl)-3-(4-chlorophenyl)-1,2,4-oxadiazole (30) (General Procedure A).** $^1$H-NMR (400 MHz; $CDCl_3$) δ 2.42-2.49 (m, 2H, $CH_2CH_2CH_2Br$), 3.15-3.19 (t, *J* = 7.2 Hz, 2H, $CH_2CH_2CH_2Br$), 3.57-3.61 (t, *J* = 6.4 Hz, 2H, $CH_2CH_2CH_2Br$), 7.47-7.49 (d, *J* = 8.4 Hz, 2H, C*H* benzene ring), 8.02-8.04 (d, *J* = 8.4 Hz, 2H, C*H* benzene ring). MS (ESI), m/z: 301 $[M + H]^+$.

**5-(3-Bromopropyl)-3-(3-chlorophenyl)-1,2,4-oxadiazole (31) (General Procedure A).** $^1$H-NMR (400 MHz; $CDCl_3$) δ 2.38-2.49 (m, 2H, $CH_2CH_2CH_2Br$), 3.15-3.19 (t, *J* = 7.2 Hz, 2H, $CH_2CH_2CH_2Br$), 3.57-3.60 (t, *J* = 6.4 Hz, 2H, $CH_2CH_2CH_2Br$), 7.41-7.50 (m, 2H, C*H* benzene ring), 7.96-7.98 (m, 1H, C*H* benzene ring), 8.08 (s, 1H, C*H* benzene ring). MS (ESI), m/z: 301 $[M + H]^+$

**5-(3-Bromopropyl)-3-(2-chlorophenyl)-1,2,4-oxadiazole (32) (General Procedure A).** $^1$H-NMR (400 MHz; $CDCl_3$) δ 2.43-2.50 (m, 2H, $CH_2CH_2CH_2Br$), 3.18-3.21 (t, *J* = 7.2 Hz, 2H, $CH_2CH_2CH_2Br$), 3.57-3.60 (t, *J* = 6.4 Hz, 2H, $CH_2CH_2CH_2Br$), 7.38-7.47 (m, 2H, C*H* benzene ring), 7.54-7.56 (m, 1H, C*H* benzene ring), 7.91-7.93 (m, 1H, C*H* benzene ring). MS (ESI), m/z: 301 $[M + H]^+$.

**5-(3-Bromopropyl)-3-phenyl-1,2,4-oxadiazole (33) (General Procedure A).** $^1$H-NMR (400 MHz; $CDCl_3$) δ 2.44-2.50 (m, 2H, $CH_2CH_2CH_2Br$), 3.14-3.19 (t, *J* = 7.2 Hz, 2H, $CH_2CH_2CH_2Br$), 3.58-3.61 (t, *J* = 6.4 Hz, 2H, $CH_2CH_2CH_2Br$), 7.49-7.51 (m, 3H, C*H* benzene ring), 8.08-8.10 (m, 2H, C*H* benzene ring). MS (ESI), m/z: 267 $[M + H]^+$.

**5-(3-Bromopropyl)-3-(4-tolyl)-1,2,4-oxadiazole (34) (General Procedure A).** $^1$H-NMR (400 MHz; $CDCl_3$) δ 2.43-2.49 (m, 5H, C*H*$_3$ and $CH_2CH_2CH_2Br$), 3.14-3.17 (t, *J* = 7.2 Hz, 2H, $CH_2CH_2CH_2Br$), 3.57-3.60 (t, *J* = 6.4 Hz, 2H, $CH_2CH_2CH_2Br$), 7.28-7.31 (d, *J* = 8.0 Hz, 2H, C*H*

benzene ring), 7.96-7.98 (d, *J* = 8.0 Hz, 2H, C*H* benzene ring). MS (ESI), m/z: 281 $[M + H]^+$.

**5-(3-Bromopropyl)-3-(4-methoxyphenyl)-1,2,4-oxadiazole (35) (General Procedure A).** $^1$H-NMR (400 MHz; $CDCl_3$) δ 2.42-2.49 (m, 2H, $CH_2CH_2CH_2Br$), 3.13-3.17 (t, *J* = 7.2 Hz, 2H, $CH_2CH_2CH_2Br$), 3.57-3.60 (t, *J* = 6.4 Hz, 2H, $CH_2CH_2CH_2Br$), 3.89 (s, 3H, $OCH_3$), 6.99-7.02 (d, *J* = 8.8 Hz, 2H, C*H* benzene ring), 8.01-8.04 (d, *J* = 8.8 Hz, 2H, C*H* benzene ring). MS (ESI), m/z: 297 $[M + H]^+$.

**5-(3-Bromopropyl)-3-(4-(trifluoromethyl)phenyl)-1,2,4-oxadiazole (36) (General Procedure A).** $^1$H-NMR (400 MHz; $CDCl_3$) δ 2.40-2.51 (m, 2H, $CH_2CH_2CH_2Br$), 3.17-3.22 (t, *J* = 7.2 Hz, 2H, $CH_2CH_2CH_2Br$), 3.58-3.62 (t, *J* = 6.4 Hz, 2H, $CH_2CH_2CH_2Br$), 7.76-7.78 (d, *J* = 8.0 Hz, 2H, C*H* benzene ring), 8.21-8.23 (d, *J* = 8.0 Hz, 2H, C*H* benzene ring). MS (ESI), m/z: 335 $[M + H]^+$.

**5-(3-Bromopropyl)-3-(4-nitrophenyl)-1,2,4-oxadiazole (37) (General Procedure A).** $^1$H-NMR (400 MHz; $CDCl_3$) δ 2.45-2.52 (m, 2H, $CH_2CH_2CH_2Br$), 3.19-3.23 (t, *J* = 7.2 Hz, 2H, $CH_2CH_2CH_2Br$), 3.59-3.62 (t, *J* = 6.4 Hz, 2H, $CH_2CH_2CH_2Br$), 8.28-8.30 (d, *J* = 7.2 Hz, 2H, C*H* benzene ring), 8.35-8.38 (d, *J* = 7.2 Hz, 2H, CH benzene ring). MS (ESI), m/z: 312 $[M + H]^+$.

**5-(3-Bromopropyl)-3-(4-fluorophenyl)-1,2,4-oxadiazole (38) (General Procedure A).** $^1$H-NMR (400 MHz; $CDCl_3$) δ 2.42-2.49 (m, 2H, $CH_2CH_2CH_2Br$), 3.15-3.18 (t, *J* = 7.2 Hz, 2H, $CH_2CH_2CH_2Br$), 3.57-3.61 (t, *J* = 6.4 Hz, 2H, $CH_2CH_2CH_2Br$), 7.16-7.21 (m, 2H, C*H* benzene ring), 8.07-8.11 (m, 2H, C*H* benzene ring). MS (ESI), m/z: 285 $[M + H]^+$.

**3-(4-Bromophenyl)-5-(3-bromopropyl)-1,2,4-oxadiazole (39) (General Procedure A).** $^1$H-NMR (400 MHz; $CDCl_3$) δ 2.43-2.49 (m, 2H, $CH_2CH_2CH_2Br$), 3.15-3.19 (t, *J* = 7.2 Hz, 2H, $CH_2CH_2CH_2Br$), 3.57-3.61 (t, *J* = 6.4 Hz, 2H, $CH_2CH_2CH_2Br$), 7.63-7.65 (d, *J* = 8.8 Hz, 2H, C*H* benzene ring), 7.95-7.97 (d, *J* = 8.8 Hz, 2H, C*H* benzene ring). MS (ESI), m/z: 347 $[M + H]^+$.

**3-(3-Bromophenyl)-5-(3-bromopropyl)-1,2,4-oxadiazole (40) (General Procedure A).** $^1$H-NMR (400 MHz; $CDCl_3$) δ 2.45-2.48 (m, 2H, $CH_2CH_2CH_2Br$), 3.16-3.20 (t, *J* = 7.2 Hz, 2H,

C*H*$_2$CH$_2$CH$_2$Br), 3.58-3.61 (t, *J* = 6.4 Hz, 2H, CH$_2$CH$_2$C*H*$_2$Br), 7.36-7.40 (t, 1H, C*H* benzene ring), 7.64-7.66 (m, 1H, C*H* benzene ring), 8.02-8.04 (m, 1H, C*H* benzene ring), 8.25 (m, 1H, C*H* benzene ring). MS (ESI), m/z: 347 $[M+H]^+$.

**3-(2-Bromophenyl)-5-(3-bromopropyl)-1,2,4-oxadiazole (41) (General Procedure A).** $^1$H-NMR (400 MHz; $CDCl_3$) δ 2.38-2.56 (m, 2H CH$_2$C*H*$_2$CH$_2$Br), 3.19-3.22 (t, *J* = 7.2 Hz, 2H, C*H*$_2$CH$_2$CH$_2$Br), 3.56-3.68 (t, *J* = 6.4 Hz, 2H, CH$_2$CH$_2$C*H*$_2$Br), 7.35-7.39 (m, 1H, C*H* benzene ring), 7.43-7.47 (m, 1H, C*H* benzene ring), 7.75-7.76 (m, 1H, C*H* benzene ring), 7.82-7.84 (m, 1H, C*H* benzene ring). MS (ESI), m/z: 347 $[M + H]^+$.

**3-(4-Bromophenyl)-5-(3-chloropropyl)-1,2,4-oxadiazole (42) (General Procedure A).** $^1$H-NMR (400 MHz; $CDCl_3$) δ 2.36-2.41 (m, 2H, CH$_2$C*H*$_2$CH$_2$Cl), 3.15-3.19 (t, *J* = 7.2 Hz, 2H, C*H*$_2$CH$_2$CH$_2$Cl), 3.71-3.75 (t, *J* = 6.4 Hz, 2H, CH$_2$CH$_2$C*H*$_2$Cl), 7.63-7.65 (d, *J* = 8.4 Hz, 2H, C*H* benzene ring), 7.95-7.97 (d, *J* = 8.4 Hz, 2H, C*H* benzene ring). MS (ESI), m/z: 301 $[M + H]^+$.

**5-(4-Bromobutyl)-3-(4-bromophenyl)-1,2,4-oxadiazole (43) (General Procedure A).** $^1$H-NMR (400 MHz; $CDCl_3$) δ 2.02-2.09 (m, 4H, CH$_2$C*H*$_2$C*H*$_2$CH$_2$Br), 2.99-3.03 (t, *J* = 7.2 Hz, 2H, C*H*$_2$CH$_2$CH$_2$CH$_2$Br), 3.47-3.62 (t, *J* = 6.4 Hz, 2H, CH$_2$CH$_2$CH$_2$C*H*$_2$Br), 7.63-7.65 (d, *J* = 8.8 Hz, 2H, C*H* benzene ring), 7.95-7.97 (d, *J* = 8.8 Hz, 2H, C*H* benzene ring). MS (ESI), m/z: 361 $[M + H]^+$.

**Preparation of Methyl 3-(4-Bromophenyl)-1,2,4-oxadiazole-5-carboxylate (44).** Methyl 2-chloro-2-oxoacetate (0.26 mL, 341.8 mg, 2.79 mmol) was added dropwise at 0 °C to a solution of (*Z*)-4-bromo-*N*'-hydroxybenzimidamide **47g** (500 mg, 2.32 mmol) in a mixture of dry dichloromethane (10 mL) and dry pyridine (1 mL). After 20 h of stirring at room temperature, the solvent was evaporated under vacuum, and the crude was triturated with water (10 mL), filtered, dried under vacuum, and finally purified by a silica gel flash chromatography (SNAP 50 KP-Sil, Biotage Isolera One) using a linear gradient of ethyl acetate (1% to 7%) in petroleum ether to give

**44**. Yield: 52%. $^1$H-NMR (400 MHz; $CDCl_3$) δ 4.13 (s, 3H, COOC*H*$_3$), 7.66-7.68 (d, *J* = 8.4 Hz, 2H, C*H* benzene ring), 8.03-8.05 (d, *J* = 8.4 Hz, 2H, C*H* benzene ring). MS (ESI), m/z: 283 $[M + H]^+$.

**Preparation of 3-(4-Bromophenyl)-5-(trifluoromethyl)-1,2,4-oxadiazole (45)**. A solution of 2,2,2-trifluoroacetic anhydride (0.39 mL, 586 mg, 2.79 mmol) in dry dichloromethane (3 mL) was added dropwise at 0 °C to a solution of (*Z*)-4-bromo-*N*'-hydroxybenzimidamide **47g** (300 mg, 1.39 mmol) in a mixture of dry dichloromethane (3 mL) and dry pyridine (0.6 mL). The reaction mixture was then stirred at room temperature for 4 h. In order to get the complete disappearance of the starting material a further addition of 2,2,2-trifluoroacetic anhydride (0.39 mL, 586 mg, 2.79 mmol) and dry pyridine (0.6 mL) was performed and the temperature of the reaction was raised up to reflux (70 °C set temperature of the oil bath) and further stirred for 22 h. After the completion of the reaction, the solvent was evaporated and the crude was triturated with water (10 mL), filtered, dried under vacuum, and finally purified by a silica gel column eluting with petroleum ether to give the pure compound **45**. Yield: 75%. $^1$H-NMR (400 MHz; $CDCl_3$) δ 7.68-7.70 (d, *J* = 8.4 Hz, 2H, C*H* benzene ring), 8.00-8.02 (d, *J* = 8.4 Hz, 2H, C*H* benzene ring). MS (ESI), m/z: 293 $[M + H]^+$.

**Preparation of 3-(4-Bromophenyl)-1,2,4-oxadiazole-5-carboxamide (46).** An excess of 7 M ammonia solution in methanol (2.2 mL, 15.57 mmol) was added to a solution of the methyl 3-(4-bromophenyl)-1,2,4-oxadiazole-5-carboxylate **44** (146.9 mg, 0.518 mmol) in methanol (8 mL), and the resulting mixture was stirred at room temperature for 2.5 h. After the disappearance of the starting material, the solvent was evaporated and the crude solid was triturated with cyclohexane, filtered and washed with cyclohexane and petroleum ether, to give pure **46** as a white solid. Yield: 65%. $^1$H-NMR (400 MHz; DMSO) δ 7.82-7.84 (d, *J* = 8.4 Hz, 2H, C*H* benzene ring), 7.98-8.00 (d, *J* = 8.4 Hz, 2H, C*H* benzene ring), 8.46 (bs, 1H, CONH*H*), 8.79 (bs, 1H, CON*H*H). MS (ESI), m/z: 268 $[M + H]^+$.

**Recombinant Expression of the Sirtuin Isoforms.** The catalytic domain of human Sirt2 (residue 43 to 356) was cloned in a pET19 derived plasmid and overexpressed in *E. coli* codon + as a fusion protein with a N-terminal His6-SUMO tag. The purification was performed as previously described.[38] Human Sirt1-Full-length, Sirt3 [114-380] and Sirt5 [34-302] were recombinantly produced in *E. coli* and purified as previously described.[40, 49, 56]

**Coupled Enzymatic Deacetylation Assay.** The deacetylase activity of Sirt2 was assayed using a described coupled enzymatic reaction.[56-57] Briefly, nicotinamidase (pNCA) and L-glutamate dehydrogenase (GDH), stoechiometrically convert the sirtuin product nicotinamide to ammonium and incorporate it into L-glutamine. The associated oxidation of NADPH to $NADP^+$ is monitored spectrophotometrically at 340 nm. Our Sirt2 reaction mixture contained 5 μg pNCA, 10.5 μg GDH (~0.5 unit), 1.75 mM α-ketoglutarate and 0.5 mM NADPH in 20 mM Na-phosphate pH 7.8 buffer and 3% DMSO. The concentration of Sirt2 was 0.8 μM. The substrate, an octameric peptide flanking the acetylated Lys40 of α-tubulin (MPSD*ac*KTIG), was used at 250 μM, and the co-substrate $NAD^+$ at 1 mM. The reaction was monitored at 20 °C for 45 min in a microplate spectrophotometer MQX200 (MWG Biotech, Germany). The background activity was measured omitting either the peptide substrate or the $NAD^+$ from the reaction. For testing inhibitors against Sirt1, Sirt3 and Sirt5 (deacetylase and desuccinylase activity) the same assay mixture was used. To obtain an activity comparable to the Sirt2 assays, Sirt1, Sirt3 and Sirt5 (deacetylase and desuccinylase activity) were used at 2, 5, 2 and 10 μM concentration, respectively, with the peptides p53 (RHK***ac*K**LMFK), AceCS2 (TRSG***ac*K**VMR), CPS1 (FKRGVL***ac*K**EYGVKV) and Prx1 (SKEYFS***succ*K**QK) as their respective substrates. For $IC_{50}$ determination, inhibitor titrations were performed in presence of 250 μM MPSD*ac*KTIG peptide and 500 μM $NAD^+$. The mechanism of

inhibition was determined by titrating either MPSD*ac*KTIG peptide or $NAD^+$ at five inhibitor concentrations (0, 0.625, 1.25, 2.5 and 5 μM). The concentration of the other, (co)substrate, was kept constant at either 250 or 500 μM for the substrate peptide and $NAD^+$, respectively. All values are averages of a minimum of four independent measurements. Analysis of the data was performed using GraFit (Erathicus Software).

**Crystallization, Diffraction Data Collection, Structure Refinement and Analysis.** Crystals of a complex between Sirt2 and ADP-ribose (ADPr) were produced as previously described.[51] In brief, Sirt2 at 11 mg/mL was co-crystallized with 20 mM ADPr using vapor diffusion method at 20 °C. Crystals of a typical size of 0.2 × 0.2 × 0.3 $mm^3$ grew within 3 to 5 days with reservoir containing 15-18 % PEG 10,000, 0.1M ammonium acetate, and 0.1M Bis-Tris pH 5.8, and drops mixed in a 1 to 3 ratio (protein/well). Crystals were soaked for 4 h in a solution composed of the mother liquor supplemented with 10 mM of **30** (10% final DMSO) containing **48** as a hydrolysis product from pre-treatment of the solution by heating to 50 °C, freeze-thawing, and sonication for 1 h. Soaked crystals were flash-frozen in liquid nitrogen after a short incubation in the soaking solution supplemented with 20% glycerol.

Diffraction data were collected on BL14.1 operated by the Helmholtz-Zentrum Berlin (HZB) at the BESSY II electron storage ring (Berlin-Adlershof, Germany)[58] at 100K using a Pilatus 6M detector and a wavelength of 0.9184 Å. The statistics of the diffraction dataset which was processed using *XDS*[59-60] within the graphical user interface provided by *XDSAPP*[61] are found in Table 2. Positional refinement was carried out using phenix.refine from the PHENIX program suite[62] and the model manually rebuilt using Coot.[63] Geometry restraints for the compounds were generated using elBOW.[64] Structural overlay were performed using the SSM algorithm in Coot. Models for **4**, **40** and **41** were generated based on the complex structure with **48** and their geometry minimized using

Phenix. Contacts within the active site were analyzed and visualized in PyMOL using show_bumps script (https://pymolwiki.org/index.php/Show_bumps). All figures were generated using the PyMOL Molecular Graphics System, version 1.7.2.1 Schrödinger, LLC.

**Cell lines and conditions.** All cell lines were grown following standard protocols. Human leukemia U937 (DSMZ-ACC5), NB4 (DSMZ-ACC207), HL-60 (DSMZ-ACC3) and K562 (DSMZ-ACC10) cells were propagated in RPMI-1640 with 10% fetal bovine serum (FBS) (Gibco), 2 mM L-glutamine (Euroclone) and antibiotics (100 U/mL penicillin, 100 µg/mL streptomycin and 250 ng/mL amphotericin-B). Human breast cancer MDA-MB-231 cells (ATCC-HTB26) were propagated in Dulbecco's Modified Eagle's Medium (DMEM), 2 mM L-glutamine (Euroclone), 10% FBS and antibiotics.

**Protein extraction and western blot analysis.** Cells were harvested and washed twice with ice-cold PBS1x. Cells were then lysed in lysis buffer (50 mM Tris-HCl pH 7.4, 150 mM NaCl, 1% NP40, 10 mM NaF, 1 mM PMSF and protease inhibitor cocktail). The lysis reaction was carried out for 15 min at 4 °C. Finally, the samples were centrifuged at 13000 rpm for 30 min at 4 °C and protein concentration quantified by Bradford assay (Bio-Rad). 50 µg of proteins were loaded on 10% polyacrylamide gels and transferred to nitrocellulose. The nitrocellulose filters were blocked in dry milk for one hour at room temperature and then was incubated with 1:500 dilution of anti-acetyl α–tubulin (Sigma). Total ERKs (Santa Cruz) were used to normalize for equal loading.

**Cell cycle analysis and apoptosis evaluation.** After the incubation with compounds, $2.5 \times 10^5$ cells were collected and resuspended in 500 µL of hypotonic buffer (0.1% Triton X-100, 0.1% sodium citrate, 50 µg/mL PI, RNAse A). Cells were incubated in the dark for 30 minutes and samples were acquired on a FACS-Calibur flow cytometer using the Cell Quest software (Becton Dickinson) and ModFitLT version 3 software (Verity). Apoptosis was measured by evaluation of the

pre-G1 content. Experiments were performed in biological duplicates and values expressed in mean ± SD.

**Cell Proliferation Assay.** Cell proliferation on different leukemia and lymphoma cell lines OCI-AML3 (DSMZ ACC-582), IMS-M2 (gift from professor B. Falini), OCI-AML2 (DSMZ, ACC-99), MV4-11 (ATCC, CRL-9591), Kasumi-1 (ATCC, CRL-2724), Karpass299 (DSMZ, ACC-31), U937 (ATCC, CRL1593.2), HL-60 (ATCC, CCL-240), NB4 (DSMZ, ACC-207) was evaluated using WST-1 assay (Roche Diagnostic GmbH Germany). The cells were plated, in triplicate, in 384-viewplate (PerkinElmer USA) at a density of $5\times10^3$ cells/well in a final volume of 22.5 µL. Cells were incubated with increasing concentrations of compounds for 48 h at 37 °C, 5% $CO_2$, then 2.5 µL of WST-1 reagent was added in each well for 1 h. For each cell line, dose-response curves were analyzed as nonlinear regression curves by using GraphPad Prism (GraphPad Software Inc.) to obtain the $IC_{50}$ values.

ASSOCIATED CONTENT

**Supporting Information**. The Supporting Information is available free of charge on the ACS Publications website at DOI: ……Supplementary Figures S1-S8. Synthesis and biochemical evaluation of **48** and **49**. Chemical and physical data of compounds **4-46**, **48** and **49.** Elemental analysis for compounds **4-46**, **48** and **49**. Molecular formula strings (CSV)

AUTHOR INFORMATION

**Corresponding Author**

A.M.: phone, +39 06 49913392; fax, +39 06 49693268; E-mail, antonello.mai@uniroma1.it.

C.S.: phone: 49 921 557830; fax: 49 921 557832; E-mail, Clemens.Steegborn@uni-bayreuth.de

D.R.: phone, +39 06 49913891; fax, +39 06 49693268; E-mail, dante.rotili@uniroma1.it

ACKNOWLEDGMENT

We thank the BESSY beamline staff for technical support. This work was supported by IIT-Sapienza Project (A.M.), by the FP7 Projects BLUEPRINT/282510 (A.M., L.A.) and A-PARADDISE/602080 (A.M.), by the COST action CM1406 Epigenetic Chemical Biology (A.M., L.A.), by AICR World Cancer Research/15-1002 (L.A.), by AIRC n°17217 (L.A.), by AIRC-TRIDEO 2015 (Id.17515) (D.R.), by PRIN 2012 (prot. 2012CTAYSY) (D.R.) and PRIN 2016 (prot. 20152TE5PK) (A.M., L.A.), and by Alzheimer Forschung Initiative eV (grant #14834) (C.S.).

ABBREVIATIONS

Ac-AceCS2, acetyl-CoA synthase 2; Ac-CPS1, carbamoyl phosphate synthetase 1; ADPr, adenosine 5'-diphosphate ribose; ALCL, anaplastic large cell lymphoma; APL, acute promyelocytic leukemia; DNMT3A, DNA methyltransferase 3A; FOXO1, forkhead box protein O1; FOXO3, forkhead box protein O3; GDH, L-glutamate dehydrogenase; H4K16, histone 4 lysine 16; H4K20, histone 4 lysine 20, HIF-1α, hypoxia-inducible factor 1-alpha; $Me_4Si$, tetramethylsilane; NPM1/ALK, nucleophosmin 1/anaplastic lymphoma kinase; pNCA, nicotinamidase; SirReal2, sirtuin 2 rearranging ligand; Suc-Prx, succinyl-peroxiredoxin-1.

**X-Ray Coordinates.** Structure factors and coordinates of the Sirt2 complex with ADP ribose and compound **48** were deposited with the Protein Data Bank (PDB; www.rcsb.org/pdb/) under accession code: 5mar. Authors will release the atomic coordinates and experimental data upon article publication.

## REFERENCES

(1) Haigis, M. C.; Sinclair, D. A. Mammalian Sirtuins: Biological Insights and Disease Relevance. *Annu. Rev. Pathol.* **2010,** *5*, 253-295.

(2) Michan, S.; Sinclair, D. Sirtuins in Mammals: Insights into Their Biological Function. *Biochem. J.* **2007,** *404* (1), 1-13.

(3) Moniot, S.; Weyand, M.; Steegborn, C. Structures, Substrates, and Regulators of Mammalian Sirtuins - Opportunities and Challenges for Drug Development. *Front. Pharmacol.* **2012,** *3*, 16.

(4) Du, J.; Zhou, Y.; Su, X.; Yu, J. J.; Khan, S.; Jiang, H.; Kim, J.; Woo, J.; Kim, J. H.; Choi, B. H.; He, B.; Chen, W.; Zhang, S.; Cerione, R. A.; Auwerx, J.; Hao, Q.; Lin, H. Sirt5 Is a Nad-Dependent Protein Lysine Demalonylase and Desuccinylase. *Science* **2011,** *334* (6057), 806-809.

(5) Feldman, J. L.; Baeza, J.; Denu, J. M. Activation of the Protein Deacetylase Sirt6 by Long-Chain Fatty Acids and Widespread Deacylation by Mammalian Sirtuins. *J. Biol. Chem.* **2013,** *288* (43), 31350-31356.

(6) Tan, M.; Peng, C.; Anderson, K. A.; Chhoy, P.; Xie, Z.; Dai, L.; Park, J.; Chen, Y.; Huang, H.; Zhang, Y.; Ro, J.; Wagner, G. R.; Green, M. F.; Madsen, A. S.; Schmiesing, J.; Peterson, B. S.; Xu, G.; Ilkayeva, O. R.; Muehlbauer, M. J.; Braulke, T.; Muhlhausen, C.; Backos, D. S.; Olsen, C. A.; McGuire, P. J.; Pletcher, S. D.; Lombard, D. B.; Hirschey, M. D.; Zhao, Y. Lysine Glutarylation Is a Protein Posttranslational Modification Regulated by Sirt5. *Cell Metab.* **2014,** *19* (4), 605-617.

(7) Houtkooper, R. H.; Pirinen, E.; Auwerx, J. Sirtuins as Regulators of Metabolism and Healthspan. *Nat. Rev. Mol. Cell Biol.* **2012,** *13* (4), 225-238.

(8) Giblin, W.; Skinner, M. E.; Lombard, D. B. Sirtuins: Guardians of Mammalian Healthspan. *Trends Genet.* **2014,** *30* (7), 271-286.

(9) Carafa, V.; Rotili, D.; Forgione, M.; Cuomo, F.; Serretiello, E.; Hailu, G. S.; Jarho, E.; Lahtela-

Kakkonen, M.; Mai, A.; Altucci, L. Sirtuin Functions and Modulation: From Chemistry to the Clinic. *Clin. Epigenetics* **2016,** *8*, 61.

(10) Cencioni, C.; Spallotta, F.; Mai, A.; Martelli, F.; Farsetti, A.; Zeiher, A. M.; Gaetano, C. Sirtuin Function in Aging Heart and Vessels. *J. Mol. Cell. Cardiol.* **2015,** *83*, 55-61.

(11) Donmez, G.; Outeiro, T. F. Sirt1 and Sirt2: Emerging Targets in Neurodegeneration. *EMBO Mol. Med.* **2013,** *5* (3), 344-352.

(12) Gizem, D. Sirtuins as Possible Targets in Neurodegenerative Diseases. *Curr. Drug Targets* **2013,** *14* (6), 644-647.

(13) Dryden, S. C.; Nahhas, F. A.; Nowak, J. E.; Goustin, A. S.; Tainsky, M. A. Role for Human Sirt2 Nad-Dependent Deacetylase Activity in Control of Mitotic Exit in the Cell Cycle. *Mol. Cell. Biol.* **2003,** *23* (9), 3173-3185.

(14) Inoue, T.; Hiratsuka, M.; Osaki, M.; Yamada, H.; Kishimoto, I.; Yamaguchi, S.; Nakano, S.; Katoh, M.; Ito, H.; Oshimura, M. Sirt2, a Tubulin Deacetylase, Acts to Block the Entry to Chromosome Condensation in Response to Mitotic Stress. *Oncogene* **2007,** *26* (7), 945-957.

(15) Wang, F.; Nguyen, M.; Qin, F. X.; Tong, Q. Sirt2 Deacetylates Foxo3a in Response to Oxidative Stress and Caloric Restriction. *Aging Cell* **2007,** *6* (4), 505-514.

(16) Wang, F.; Tong, Q. Sirt2 Suppresses Adipocyte Differentiation by Deacetylating Foxo1 and Enhancing Foxo1's Repressive Interaction with Ppargamma. *Mol. Biol. Cell* **2009,** *20* (3), 801-808.

(17) Seo, K. S.; Park, J. H.; Heo, J. Y.; Jing, K.; Han, J.; Min, K. N.; Kim, C.; Koh, G. Y.; Lim, K.; Kang, G. Y.; Uee Lee, J.; Yim, Y. H.; Shong, M.; Kwak, T. H.; Kweon, G. R. Sirt2 Regulates Tumour Hypoxia Response by Promoting Hif-1alpha Hydroxylation. *Oncogene* **2015,** *34* (11), 1354-1362.

(18) Kim, H. S.; Vassilopoulos, A.; Wang, R. H.; Lahusen, T.; Xiao, Z.; Xu, X.; Li, C.; Veenstra, T. D.; Li, B.; Yu, H.; Ji, J.; Wang, X. W.; Park, S. H.; Cha, Y. I.; Gius, D.; Deng, C. X. Sirt2

Maintains Genome Integrity and Suppresses Tumorigenesis through Regulating Apc/C Activity. *Cancer Cell* **2011,** *20* (4), 487-499.

(19) Serrano, L.; Martinez-Redondo, P.; Marazuela-Duque, A.; Vazquez, B. N.; Dooley, S. J.; Voigt, P.; Beck, D. B.; Kane-Goldsmith, N.; Tong, Q.; Rabanal, R. M.; Fondevila, D.; Munoz, P.; Kruger, M.; Tischfield, J. A.; Vaquero, A. The Tumor Suppressor Sirt2 Regulates Cell Cycle Progression and Genome Stability by Modulating the Mitotic Deposition of H4k20 Methylation. *Genes Dev.* **2013,** *27* (6), 639-653.

(20) Li, Y.; Matsumori, H.; Nakayama, Y.; Osaki, M.; Kojima, H.; Kurimasa, A.; Ito, H.; Mori, S.; Katoh, M.; Oshimura, M.; Inoue, T. Sirt2 Down-Regulation in Hela Can Induce P53 Accumulation Via P38 Mapk Activation-Dependent P300 Decrease, Eventually Leading to Apoptosis. *Genes Cells* **2011,** *16* (1), 34-45.

(21) Zhao, Y.; Yang, J.; Liao, W.; Liu, X.; Zhang, H.; Wang, S.; Wang, D.; Feng, J.; Yu, L.; Zhu, W. G. Cytosolic Foxo1 Is Essential for the Induction of Autophagy and Tumour Suppressor Activity. *Nat. Cell Biol.* **2010,** *12* (7), 665-675.

(22) Liu, P. Y.; Xu, N.; Malyukova, A.; Scarlett, C. J.; Sun, Y. T.; Zhang, X. D.; Ling, D.; Su, S. P.; Nelson, C.; Chang, D. K.; Koach, J.; Tee, A. E.; Haber, M.; Norris, M. D.; Toon, C.; Rooman, I.; Xue, C.; Cheung, B. B.; Kumar, S.; Marshall, G. M.; Biankin, A. V.; Liu, T. The Histone Deacetylase Sirt2 Stabilizes Myc Oncoproteins. *Cell Death Differ.* **2013,** *20* (3), 503-514.

(23) Jing, H.; Hu, J.; He, B.; Negron Abril, Y. L.; Stupinski, J.; Weiser, K.; Carbonaro, M.; Chiang, Y. L.; Southard, T.; Giannakakou, P.; Weiss, R. S.; Lin, H. A Sirt2-Selective Inhibitor Promotes C-Myc Oncoprotein Degradation and Exhibits Broad Anticancer Activity. *Cancer Cell* **2016,** *29* (5), 767-768.

(24) Yang, M. H.; Laurent, G.; Bause, A. S.; Spang, R.; German, N.; Haigis, M. C.; Haigis, K. M. Hdac6 and Sirt2 Regulate the Acetylation State and Oncogenic Activity of Mutant K-Ras. *Mol.*

*Cancer Res.* **2013,** *11* (9), 1072-1077.

(25) McGlynn, L. M.; Zino, S.; MacDonald, A. I.; Curle, J.; Reilly, J. E.; Mohammed, Z. M.; McMillan, D. C.; Mallon, E.; Payne, A. P.; Edwards, J.; Shiels, P. G. Sirt2: Tumour Suppressor or Tumour Promoter in Operable Breast Cancer? *Eur. J. Cancer* **2014,** *50* (2), 290-301.

(26) Xu, H.; Li, Y.; Chen, L.; Wang, C.; Wang, Q.; Zhang, H.; Lin, Y.; Li, Q.; Pang, T. Sirt2 Mediates Multidrug Resistance in Acute Myelogenous Leukemia Cells Via Erk1/2 Signaling Pathway. *Int. J. Oncol.* **2016,** *48* (2), 613-623.

(27) Deng, A.; Ning, Q.; Zhou, L.; Liang, Y. Sirt2 Is an Unfavorable Prognostic Biomarker in Patients with Acute Myeloid Leukemia. *Sci. Rep.* **2016,** *6*, 27694.

(28) Outeiro, T. F.; Kontopoulos, E.; Altmann, S. M.; Kufareva, I.; Strathearn, K. E.; Amore, A. M.; Volk, C. B.; Maxwell, M. M.; Rochet, J. C.; McLean, P. J.; Young, A. B.; Abagyan, R.; Feany, M. B.; Hyman, B. T.; Kazantsev, A. G. Sirtuin 2 Inhibitors Rescue Alpha-Synuclein-Mediated Toxicity in Models of Parkinson's Disease. *Science* **2007,** *317* (5837), 516-519.

(29) Taylor, D. M.; Balabadra, U.; Xiang, Z.; Woodman, B.; Meade, S.; Amore, A.; Maxwell, M. M.; Reeves, S.; Bates, G. P.; Luthi-Carter, R.; Lowden, P. A.; Kazantsev, A. G. A Brain-Permeable Small Molecule Reduces Neuronal Cholesterol by Inhibiting Activity of Sirtuin 2 Deacetylase. *ACS Chem. Biol.* **2011,** *6* (6), 540-546.

(30) Quinti, L.; Casale, M.; Moniot, S.; Pais, T. F.; Van Kanegan, M. J.; Kaltenbach, L. S.; Pallos, J.; Lim, R. G.; Naidu, S. D.; Runne, H.; Meisel, L.; Rauf, N. A.; Leyfer, D.; Maxwell, M. M.; Saiah, E.; Landers, J. E.; Luthi-Carter, R.; Abagyan, R.; Dinkova-Kostova, A. T.; Steegborn, C.; Marsh, J. L.; Lo, D. C.; Thompson, L. M.; Kazantsev, A. G. Sirt2- and Nrf2-Targeting Thiazole-Containing Compound with Therapeutic Activity in Huntington's Disease Models. *Cell Chem. Biol.* **2016,** *23* (7), 849-861.

(31) Rumpf, T.; Schiedel, M.; Karaman, B.; Roessler, C.; North, B. J.; Lehotzky, A.; Olah, J.;

Ladwein, K. I.; Schmidtkunz, K.; Gajer, M.; Pannek, M.; Steegborn, C.; Sinclair, D. A.; Gerhardt, S.; Ovadi, J.; Schutkowski, M.; Sippl, W.; Einsle, O.; Jung, M. Selective Sirt2 Inhibition by Ligand-Induced Rearrangement of the Active Site. *Nat. Commun.* **2015,** *6*, 6263.

(32) Schiedel, M.; Rumpf, T.; Karaman, B.; Lehotzky, A.; Olah, J.; Gerhardt, S.; Ovadi, J.; Sippl, W.; Einsle, O.; Jung, M. Aminothiazoles as Potent and Selective Sirt2 Inhibitors: A Structure-Activity Relationship Study. *J. Med. Chem.* **2016,** *59* (4), 1599-1612.

(33) Seifert, T.; Malo, M.; Kokkola, T.; Engen, K.; Friden-Saxin, M.; Wallen, E. A.; Lahtela-Kakkonen, M.; Jarho, E. M.; Luthman, K. Chroman-4-One- and Chromone-Based Sirtuin 2 Inhibitors with Antiproliferative Properties in Cancer Cells. *J. Med. Chem.* **2014,** *57* (23), 9870-9888.

(34) Sakai, T.; Matsumoto, Y.; Ishikawa, M.; Sugita, K.; Hashimoto, Y.; Wakai, N.; Kitao, A.; Morishita, E.; Toyoshima, C.; Hayashi, T.; Akiyama, T. Design, Synthesis and Structure-Activity Relationship Studies of Novel Sirtuin 2 (Sirt2) Inhibitors with a Benzamide Skeleton. *Bioorg. Med. Chem.* **2015,** *23* (2), 328-339.

(35) Suzuki, T.; Khan, M. N.; Sawada, H.; Imai, E.; Itoh, Y.; Yamatsuta, K.; Tokuda, N.; Takeuchi, J.; Seko, T.; Nakagawa, H.; Miyata, N. Design, Synthesis, and Biological Activity of a Novel Series of Human Sirtuin-2-Selective Inhibitors. *J. Med. Chem.* **2012,** *55* (12), 5760-5773.

(36) Cui, H.; Kamal, Z.; Ai, T.; Xu, Y.; More, S. S.; Wilson, D. J.; Chen, L. Discovery of Potent and Selective Sirtuin 2 (Sirt2) Inhibitors Using a Fragment-Based Approach. *J. Med. Chem.* **2014,** *57* (20), 8340-8357.

(37) Ai, T.; Wilson, D. J.; More, S. S.; Xie, J.; Chen, L. 5-((3-Amidobenzyl)Oxy)Nicotinamides as Sirtuin 2 Inhibitors. *J. Med. Chem.* **2016,** *59* (7), 2928-2941.

(38) Di Fruscia, P.; Zacharioudakis, E.; Liu, C.; Moniot, S.; Laohasinnarong, S.; Khongkow, M.; Harrison, I. F.; Koltsida, K.; Reynolds, C. R.; Schmidtkunz, K.; Jung, M.; Chapman, K. L.;

Steegborn, C.; Dexter, D. T.; Sternberg, M. J.; Lam, E. W.; Fuchter, M. J. The Discovery of a Highly Selective 5,6,7,8-Tetrahydrobenzo[4,5]Thieno[2,3-D]Pyrimidin-4(3h)-One Sirt2 Inhibitor That Is Neuroprotective in an in Vitro Parkinson's Disease Model. *ChemMedChem* **2015,** *10* (1), 69-82.

(39) Yamagata, K.; Goto, Y.; Nishimasu, H.; Morimoto, J.; Ishitani, R.; Dohmae, N.; Takeda, N.; Nagai, R.; Komuro, I.; Suga, H.; Nureki, O. Structural Basis for Potent Inhibition of Sirt2 Deacetylase by a Macrocyclic Peptide Inducing Dynamic Structural Change. *Structure* **2014,** *22* (2), 345-352.

(40) Schlicker, C.; Boanca, G.; Lakshminarasimhan, M.; Steegborn, C. Structure-Based Development of Novel Sirtuin Inhibitors. *Aging (Albany NY)* **2011,** *3* (9), 852-872.

(41) Cottrell, D. M.; Capers, J.; Salem, M. M.; DeLuca-Fradley, K.; Croft, S. L.; Werbovetz, K. A. Antikinetoplastid Activity of 3-Aryl-5-Thiocyanatomethyl-1,2,4-Oxadiazoles. *Bioorg. Med. Chem.* **2004,** *12* (11), 2815-2824.

(42) Srivastava, R. M.; Brinn, I. M.; Machuca-Herrera, J. O.; Faria, H. B.; Carpenter, G. B.; Andrade, D.; Venkatesh, C. G.; F. de Morais, L. P. Benzamidoximes: Structural, Conformational and Spectroscopic Studies. I. *J. Mol. Struct.* **1997,** *406* (1–2), 159-167.

(43) La Motta, C.; Sartini, S.; Salerno, S.; Simorini, F.; Taliani, S.; Marini, A. M.; Da Settimo, F.; Marinelli, L.; Limongelli, V.; Novellino, E. Acetic Acid Aldose Reductase Inhibitors Bearing a Five-Membered Heterocyclic Core with Potent Topical Activity in a Visual Impairment Rat Model. *J. Med. Chem.* **2008,** *51* (11), 3182-3193.

(44) Xia, G.; You, X.; Liu, L.; Liu, H.; Wang, J.; Shi, Y.; Li, P.; Xiong, B.; Liu, X.; Shen, J. Design, Synthesis and Sar of Piperidyl-Oxadiazoles as 11beta-Hydroxysteroid Dehydrogenase 1 Inhibitors. *Eur. J. Med. Chem.* **2013,** *62*, 1-10.

(45) Wang, Z.; Zhang, H.; Jabeen, F.; Gopinathan-Pillai, G.; Arami, J. A.; Killian, B. J.; Stiegler, K. D.; Yudewitz, D. S.; Thiemann, P. L.; Turk, J. D.; Zhou, W.; Steel, P. J.; Hall, C. D.; Katritzky, A.

R. Synthesis and Properties of Energetic 1,2,4-Oxadiazoles. *Eur. J. Org. Chem.* **2015,** *2015* (34), 7468-7474.

(46) Cai, J.; Wei, H.; Hong, K. H.; Wu, X.; Cao, M.; Zong, X.; Li, L.; Sun, C.; Chen, J.; Ji, M. Discovery and Preliminary Evaluation of 2-Aminobenzamide and Hydroxamate Derivatives Containing 1,2,4-Oxadiazole Moiety as Potent Histone Deacetylase Inhibitors. *Eur. J. Med. Chem.* **2015,** *96*, 1-13.

(47) Vogel, T. M.; Reinhard, M. Reaction Products and Rates of Disappearance of Simple Bromoalkanes, 1,2-Dibromopropane, and 1,2-Dibromoethane in Water. *Environ. Sci. Technol.* **1986,** *20* (10), 992-997.

(48) Mabey, W.; Mill, T. Critical Review of Hydrolysis of Organic Compounds in Water under Environmental Conditions. *J. Phys. Chem. Ref. Data* **1978,** *7* (2), 383-415.

(49) Gertz, M.; Fischer, F.; Nguyen, G. T.; Lakshminarasimhan, M.; Schutkowski, M.; Weyand, M.; Steegborn, C. Ex-527 Inhibits Sirtuins by Exploiting Their Unique Nad+-Dependent Deacetylation Mechanism. *Proc. Natl. Acad. Sci. U. S. A.* **2013,** *110* (30), E2772-2781.

(50) Gertz, M.; Steegborn, C. Using Mitochondrial Sirtuins as Drug Targets: Disease Implications and Available Compounds. *Cell. Mol. Life Sci.* **2016,** *73* (15), 2871-2896.

(51) Rumpf, T.; Gerhardt, S.; Einsle, O.; Jung, M. Seeding for Sirtuins: Microseed Matrix Seeding to Obtain Crystals of Human Sirt3 and Sirt2 Suitable for Soaking. *Acta Crystallogr. F Struct. Biol. Commun.* **2015,** *71* (Pt 12), 1498-1510.

(52) Napper, A. D.; Hixon, J.; McDonagh, T.; Keavey, K.; Pons, J. F.; Barker, J.; Yau, W. T.; Amouzegh, P.; Flegg, A.; Hamelin, E.; Thomas, R. J.; Kates, M.; Jones, S.; Navia, M. A.; Saunders, J. O.; DiStefano, P. S.; Curtis, R. Discovery of Indoles as Potent and Selective Inhibitors of the Deacetylase Sirt1. *J. Med. Chem.* **2005,** *48* (25), 8045-8054.

(53) Gomes, P.; Outeiro, T. F.; Cavadas, C. Emerging Role of Sirtuin 2 in the Regulation of

Mammalian Metabolism. *Trends Pharmacol. Sci.* **2015,** *36* (11), 756-768.

(54) Cha, Y. I.; Kim, H.-S. Emerging Role of Sirtuins on Tumorigenesis: Possible Link between Aging and Cancer. *BMB Reports* **2013,** *46* (9), 429-438.

(55) Bosch-Presegue, L.; Vaquero, A. The Dual Role of Sirtuins in Cancer. *Genes Cancer* **2011,** *2* (6), 648-662.

(56) Suenkel, B.; Steegborn, C. Recombinant Preparation, Biochemical Analysis, and Structure Determination of Sirtuin Family Histone/Protein Deacylases. *Methods Enzymol.* **2016,** *573*, 183-208.

(57) Smith, B. C.; Hallows, W. C.; Denu, J. M. A Continuous Microplate Assay for Sirtuins and Nicotinamide-Producing Enzymes. *Anal. Biochem.* **2009,** *394* (1), 101-109.

(58) Mueller, U.; Förster, R.; Hellmig, M.; Huschmann, F. U.; Kastner, A.; Malecki, P.; Pühringer, S.; Röwer, M.; Sparta, K.; Steffien, M.; Ühlein, M.; Wilk, P.; Weiss, M. S. The Macromolecular Crystallography Beamlines at Bessy Ii of the Helmholtz-Zentrum Berlin: Current Status and Perspectives. *Eur. Phys. J. Plus* **2015,** *130* (7), 141.

(59) Kabsch, W. Integration, Scaling, Space-Group Assignment and Post-Refinement. *Acta Crystallogr. D Biol. Crystallogr.* **2010,** *66* (Pt 2), 133-144.

(60) Kabsch, W. Xds. *Acta Crystallogr. D Biol. Crystallogr.* **2010,** *66* (Pt 2), 125-132.

(61) Sparta, K. M.; Krug, M.; Heinemann, U.; Mueller, U.; Weiss, M. S. Xdsapp2.0. *J. Appl. Crystallogr.* **2016,** *49* (3), 1085-1092.

(62) Adams, P. D.; Afonine, P. V.; Bunkoczi, G.; Chen, V. B.; Davis, I. W.; Echols, N.; Headd, J. J.; Hung, L. W.; Kapral, G. J.; Grosse-Kunstleve, R. W.; McCoy, A. J.; Moriarty, N. W.; Oeffner, R.; Read, R. J.; Richardson, D. C.; Richardson, J. S.; Terwilliger, T. C.; Zwart, P. H. Phenix: A Comprehensive Python-Based System for Macromolecular Structure Solution. *Acta Crystallogr. D Biol. Crystallogr.* **2010,** *66* (Pt 2), 213-221.

(63) Emsley, P.; Lohkamp, B.; Scott, W. G.; Cowtan, K. Features and Development of Coot. *Acta Crystallogr. D Biol. Crystallogr.* **2010,** *66* (Pt 4), 486-501.

(64) Moriarty, N. W.; Grosse-Kunstleve, R. W.; Adams, P. D. Electronic Ligand Builder and Optimization Workbench (Elbow): A Tool for Ligand Coordinate and Restraint Generation. *Acta Crystallogr. D Biol. Crystallogr.* **2009,** *65* (Pt 10), 1074-1080.

## Figures and Captions

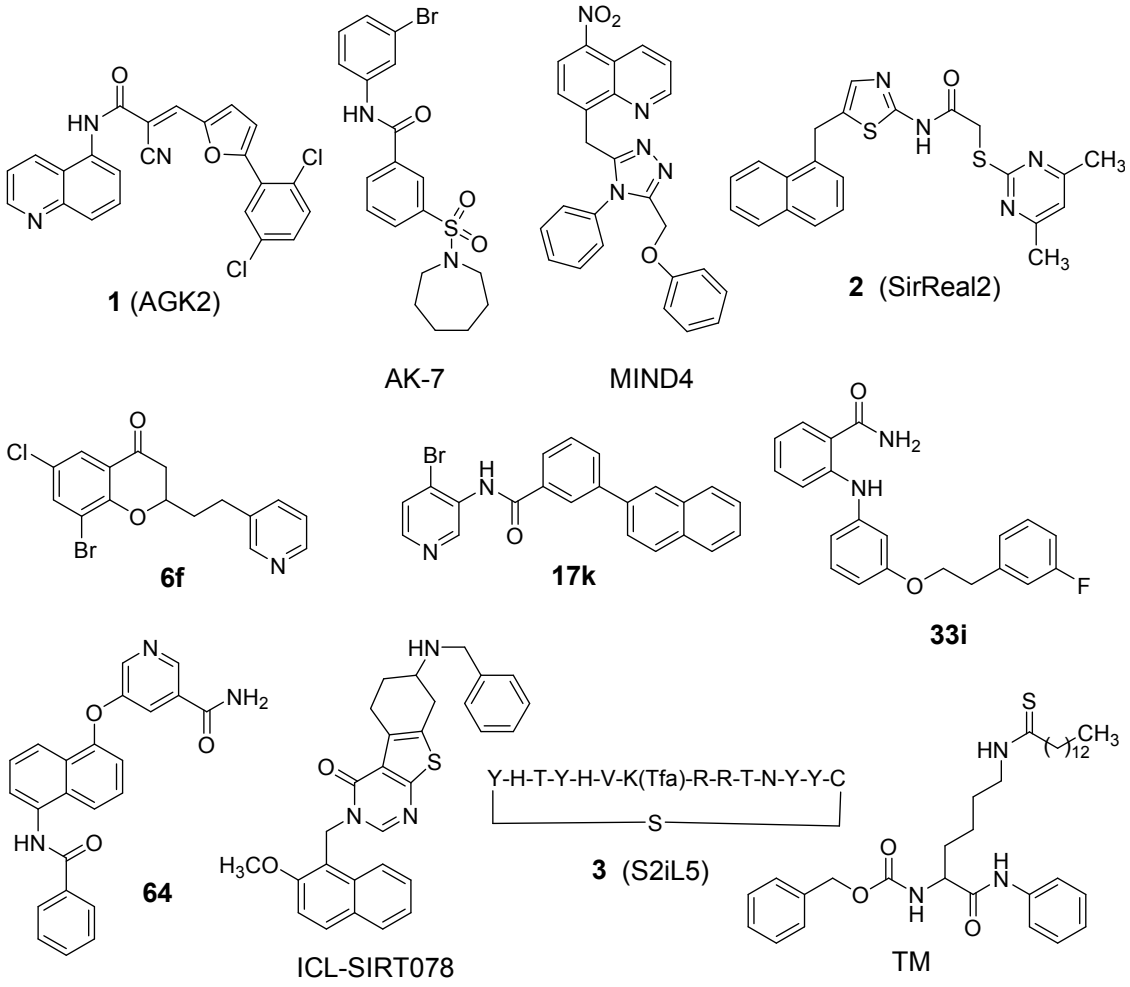


**Figure 1.** Known Sirt2-selective inhibitors.

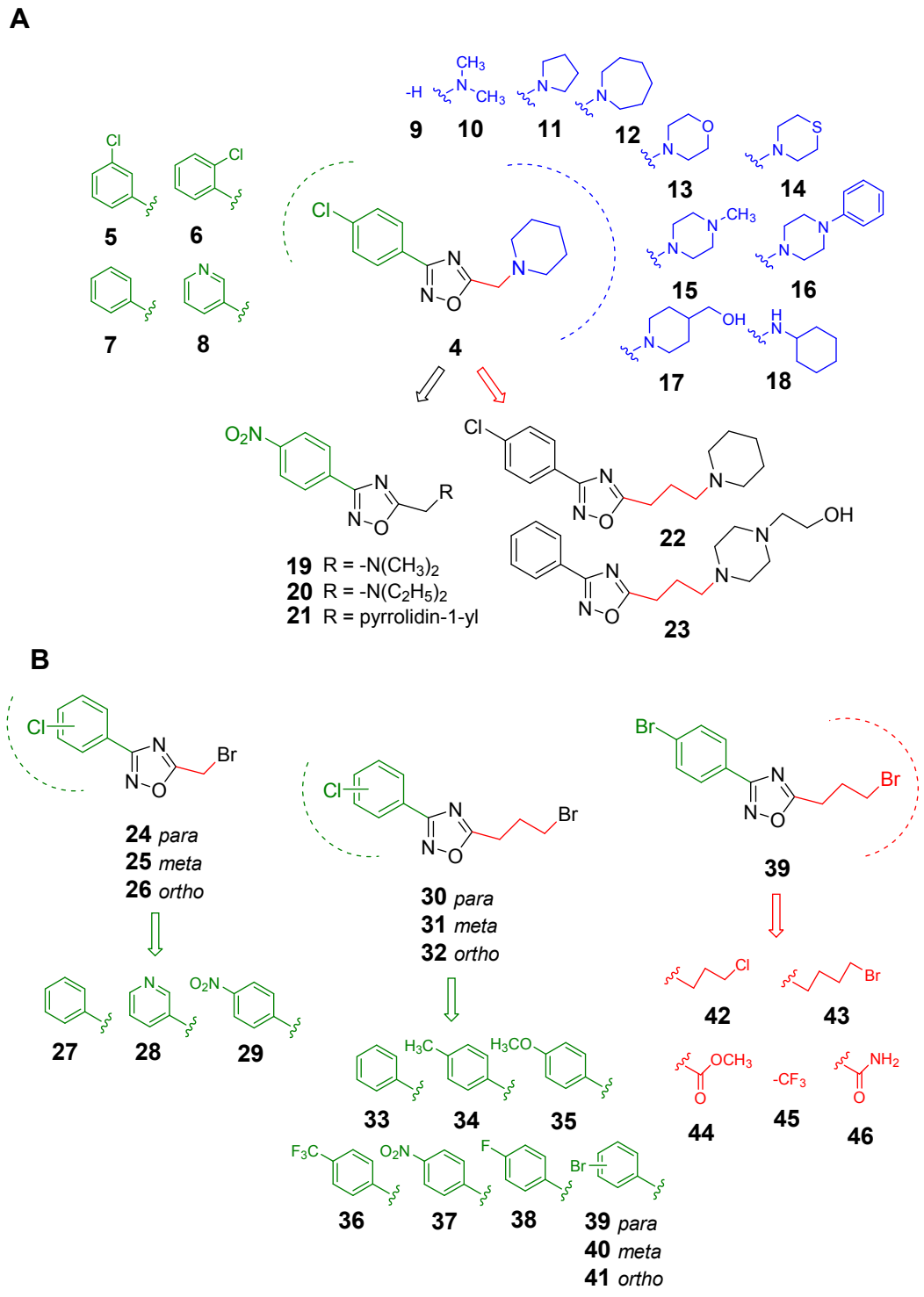


**Figure 2.** A) Chemical modifications performed on the hit compound **4**. B) Chemical modification

performed on the intermediate compounds **24**, **30** and **39**.

**Scheme 1.** Synthesis of Compounds **2-44**[a]

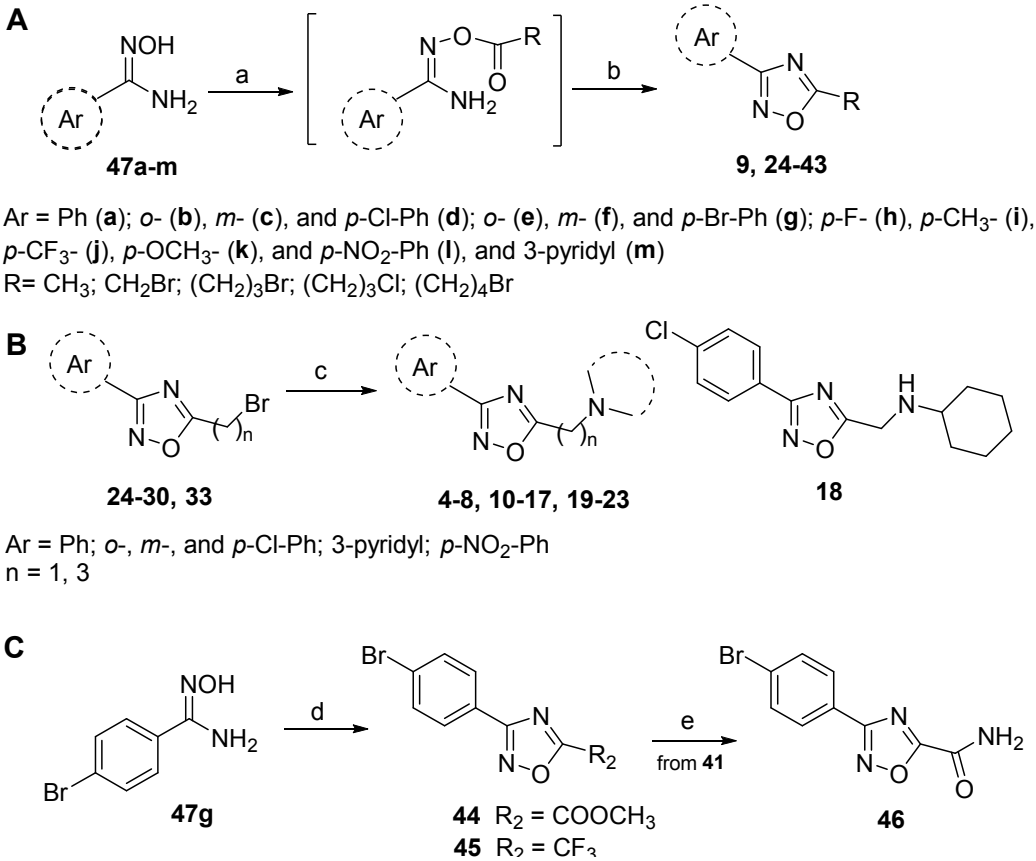


[a]Reagents and conditions: (a) appropriate acyl halide, triethylamine, dry dichloromethane, 0 °C → rt, 1-2 h, 75-85% yield; (b) toluene or *o*-xylene, reflux, 1.5-8 h, 25-76% yield; (c) appropriate (cyclic) amine, sodium iodide, $K_2CO_3$, dry DMF, 60 °C, 1-2 h, 33-89% yield; (d) methyl 2-chloro-2-oxoacetate or trifluoroacetic anhydride, dry pyridine, dry dichloromethane, 0 °C → rt or reflux, 20-22 h, 52-75% yield; (e) 7M $NH_3$ in methanol, rt, 2.5 h, 65% yield.

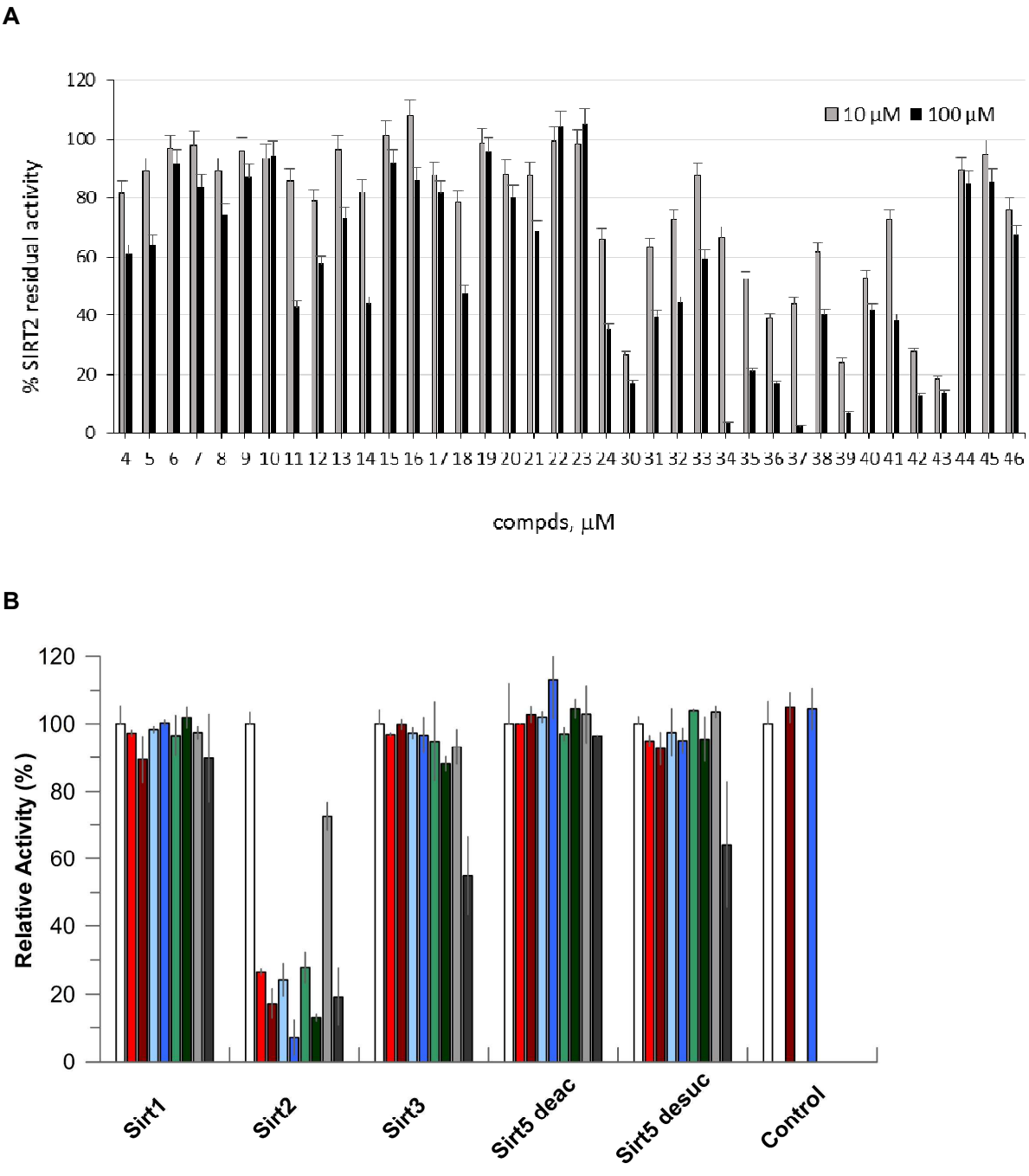


**Figure 3.** (**A**) Percentage of Sirt2 residual activity in the presence of compounds **4-24**, **30-46** tested at 10 and 100 µM. (**B**) Isoform selectivity and comparison with **1**. The activity of Sirt1, 2, 3 and 5 (deacetylase and desuccinylase) was measured in presence of either 10 (light) or 100 µM (dark) of

**30** (red), **39** (blue), **42** (green), and **1** (grey) and compared to the reference activity. For the control experiment, sirtuin was omitted from the reaction mix and nicotinamide (100 μM) was used to start the downstream reaction.

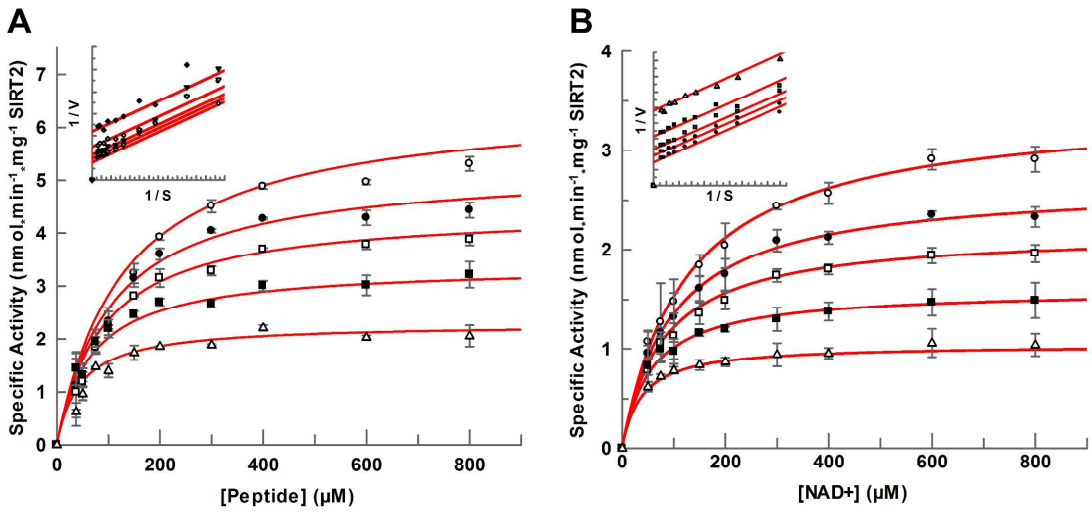


**Figure 4.** 1,2,4-Oxadiazoles are uncompetitive Sirt2 inhibitors. Competition experiment with **39** and the Sirt2 acetyl substrate (**A**) and $NAD^+$ co-substrate (**B**). Deacetylase activity of Sirt2 was measured at several concentrations of **39** (0 μM (empty circles), 0.625 μM (filled circles), 1.25 μM (empty squares), 2.5 μM (filled squares), and 5 μM (triangles). The best-fitting inhibition model is uncompetitive for both substrate and co-substrate and the corresponding fitted $K_i$ is 2.18 ± 0.04 and 2.22 ± 0.11 respectively. Inserts correspond to the Lineweaver-Burk double reciprocal transformation of the data.

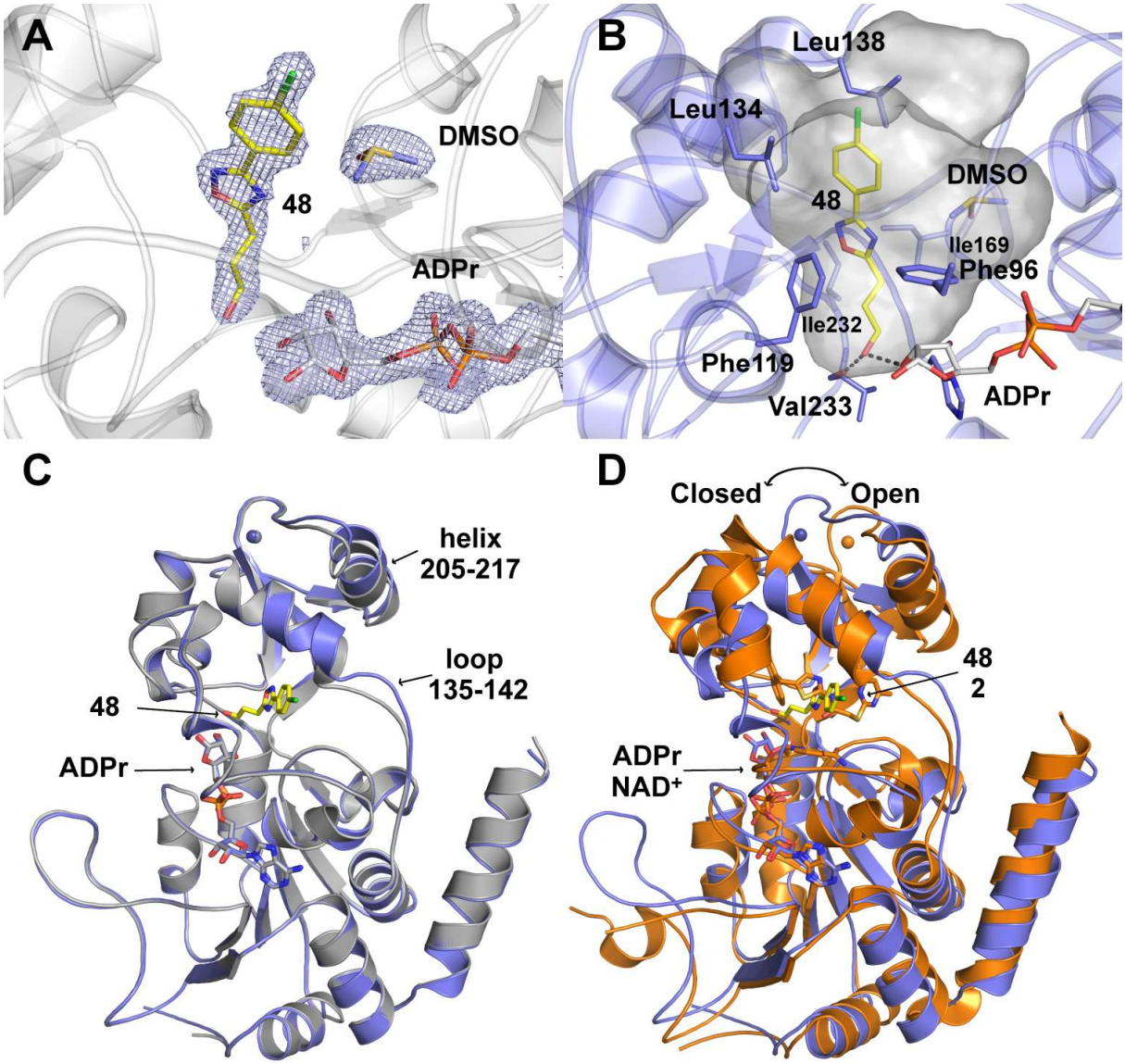


**Figure 5.** Sirt2/**48**/ADP-ribose complex and comparison with selected Sirt2 crystal structures. In all panels, overall structures are shown as cartoon with the ligands as sticks and the Zn atom as sphere. Compound **48** is colored in yellow. (**A**) Close up view of the active site of Sirt2 (white; chain A) with bound ligands represented in their 2mFo-DFc electron density (1σ contour). Compound **48**, ADPr and DMSO are show as sticks in yellow, white and blue, respectively. (**B**) Close up view of

the binding site of **48**. The protein is shown in blue with the residues of the active and inhibitor binding sites represented as sticks. The molecule of ADP-ribose is shown in white and **48** is shown in yellow in the hydrophobic cavity located at the back of Sirt2's active site. (**C**) The structure of the Sirt2/ADPr/**48** complex (blue) was superposed to the structure of the Sirt2/ADP-ribose complex (grey) (PDBid: 5d7o). The most significant conformational differences are located in the Zn-binding domain for the regions 135-142 and 205-217. (**D**) The structure of the Sirt2/ADPr/**48** complex (blue) was superposed to the structure of the Sirt2/ADPr/**2** complex (orange) (PDBid: 4rmg). The characteristic closure movement of the Zn-binding domain of Sirt2 is symbolized with a curved arrow.

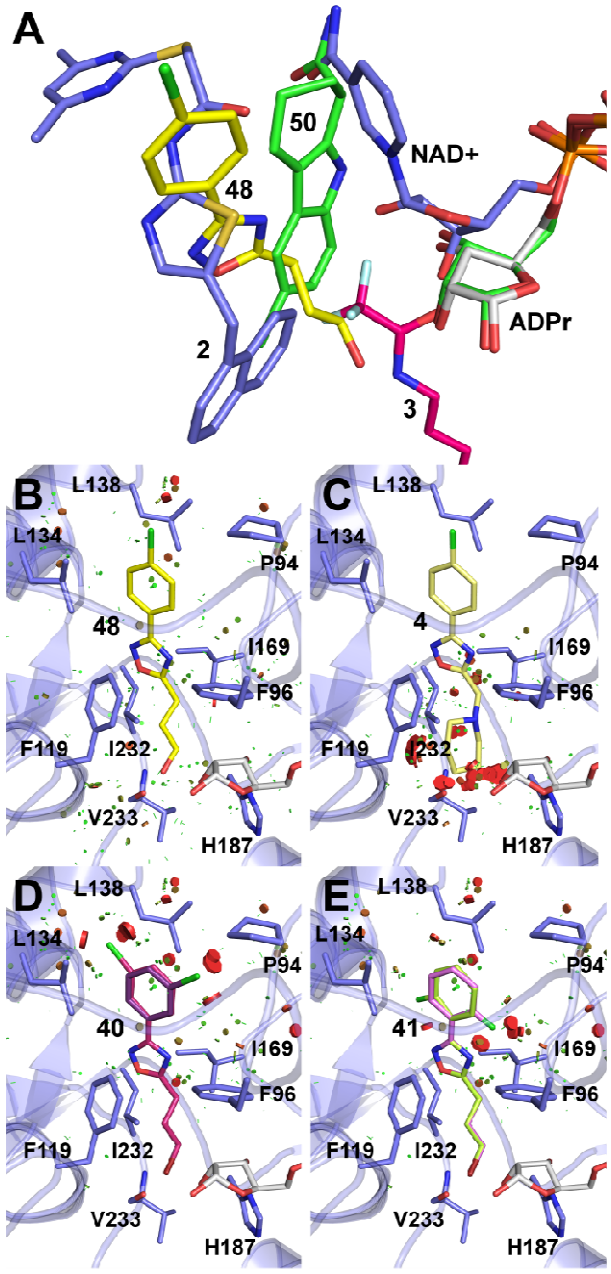


**Figure 6.** Comparison of the bound conformation of **48** with selected Sirt2 inhibitors and modelling of a set of 1,2,4-oxadiazole inhibitors in the active site of Sirt2. (**A**) The structure of the complex between Sirt2 and **2**/$NAD^+$ (PDBid: 4rmg; blue) or **50**/ADP-ribose (PDBid: 5d7p; green) or the macrocyclic trifluoroacetylated peptide **3** (PDBid: 4l3o; magenta) were superposed to the complex with **48**/ADP-ribose (yellow/white) and the ligands displayed as sticks. (**B-E**) A set of 1,2,4-

oxadiazole compounds were modelled in the active site of Sirt2 based on the complex structure with **48** (yellow in **A**). The protein (blue) is shown as cartoon with the residues of the binding site as well as the ADP-ribose (white) shown as sticks. Compounds **4** (green), **40** (pink and violet) and **41** (light pink and yellow) are depicted in panel **C**, **D** and **E** respectively. Overlapping van der Waals radii are indicated by red disk which materialize steric hindrance.

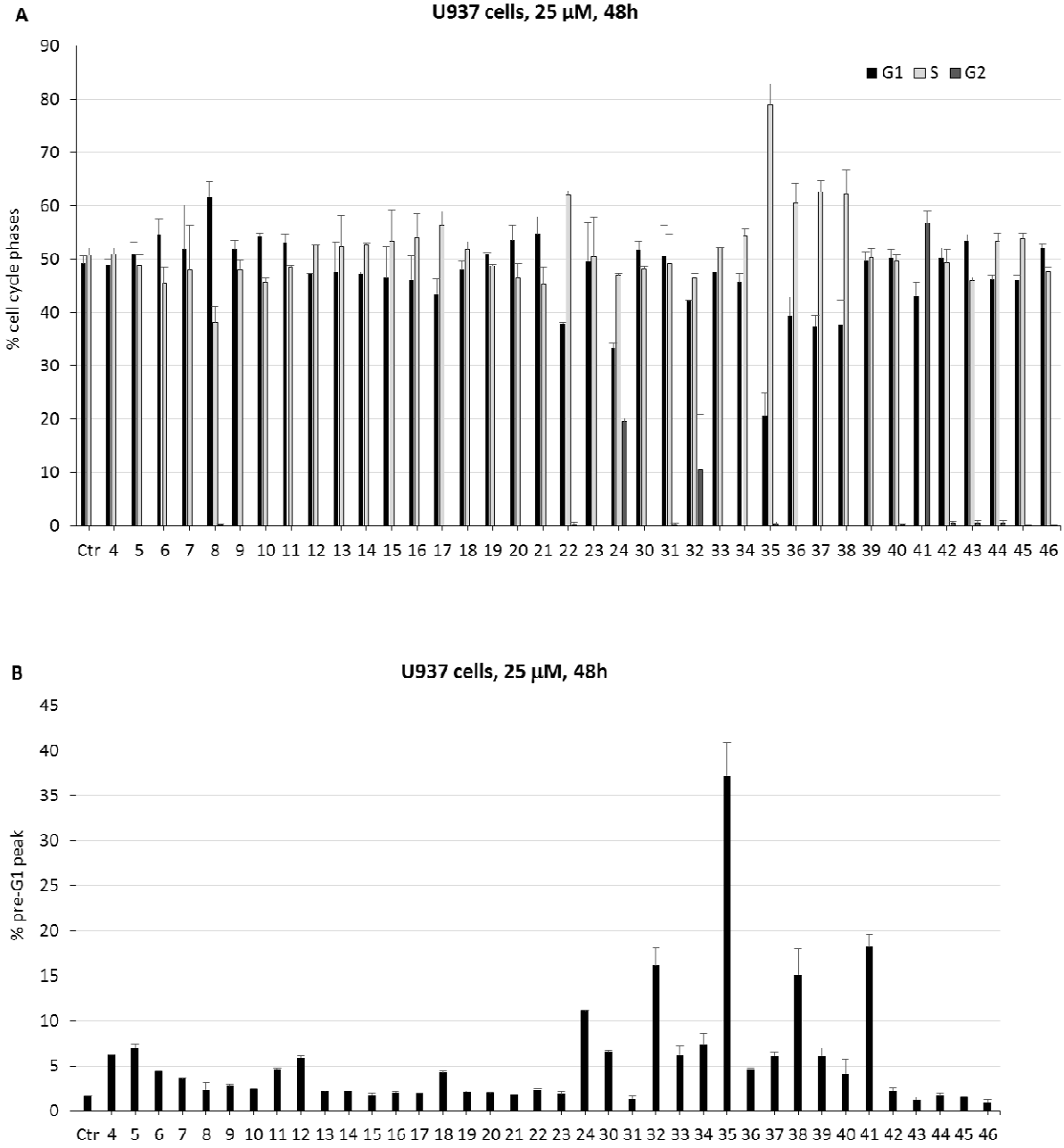


**Figure 7.** Effects on cell cycle (**A**) and apoptosis induction (**B**) of 1,2,4-oxadiazoles **4-24**, **30-46** in U937 treated with 25 µM compounds for 48 h.

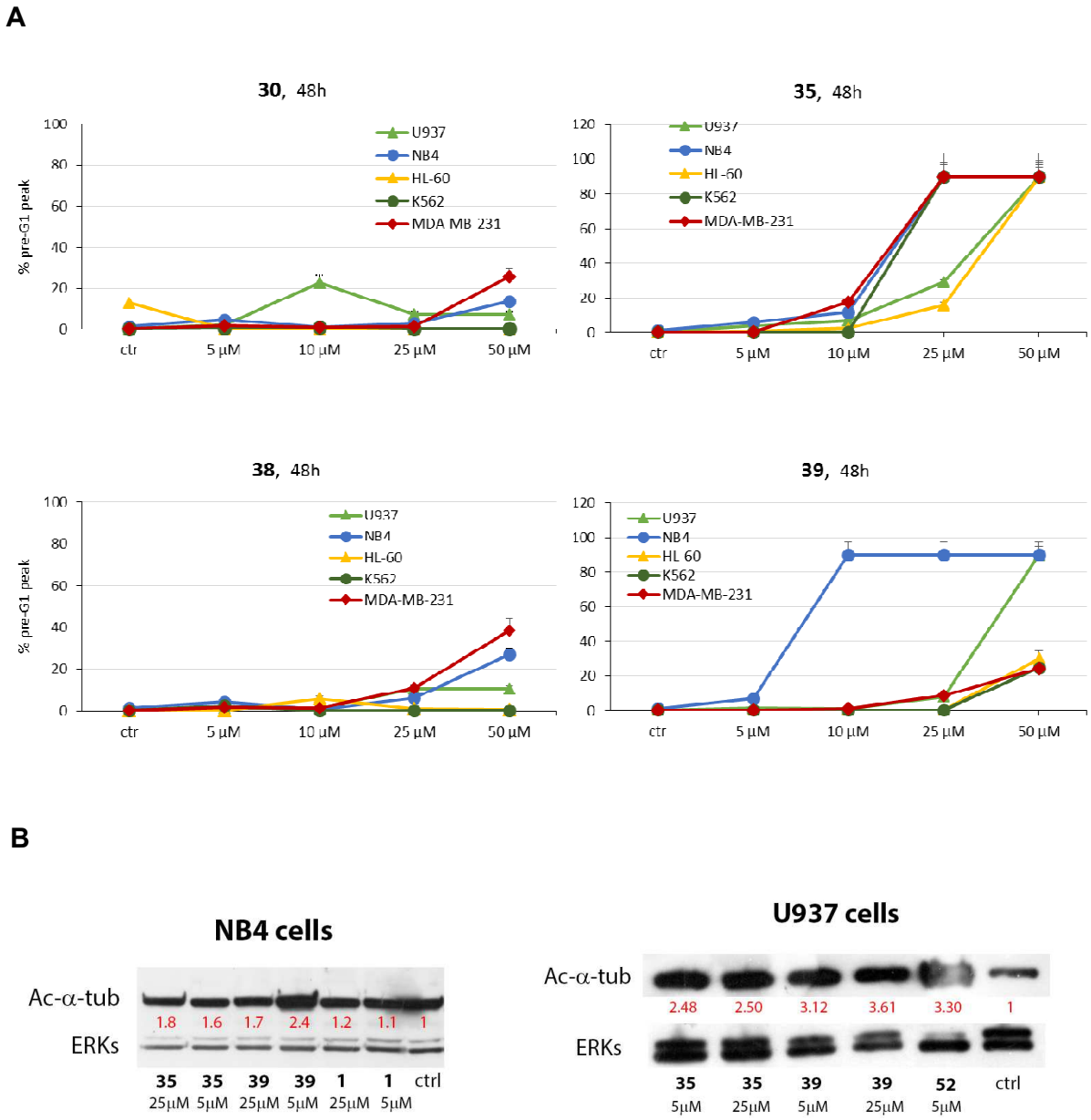


**Figure 8.** (**A**) Dose-response curves of apoptosis induction in leukemia U937, NB4, HL-60, and K562 cells and in breast cancer MDA-MB-31 cells treated with different doses of **28**, **33**, **36** and **37** for 48 h. (**B**) Western blot analyses performed on NB4 (left) and U937 (right) cells treated with **33** and **37** (5 and 25 µM) for 4 (NB4) or 24 (U937) h. Compound **1** has been added for comparison. Compound **52** has been added as a positive control. Antibodies anti-acetyl-α-tubulin have been

used. ERKs have been used for equal loading. Densitometric data have been shown in red.

# Table of Content Graphic